Processes linking wind erosion and ecosystem dynamics in a dust source hotspot in East Asia

(東アジアのダスト発生ホットスポットにおいて風食と生態系動態を結び付けるプロセス)

KONG, Kaman

(江 嘉敏)

A dissertation for the degree of Doctor of Science

Department of Earth and Environmental Sciences,

Graduate School of Environmental Studies, Nagoya University

（名古屋大学大学院環境学研究科地球環境科学専攻学位論文　博士（理学））

2021

Abstract

Wind erosion is an important environmental phenomenon in arid and semi-arid regions worldwide. It has substantial influences on human and livestock health conditions, economic activities, and ecosystem dynamics, in both the source and downwind areas. The Mongolian grasslands are a dust hotspot with the highest frequencies of dust outbreaks in East Asia and an increasing number of dust events since the 2000s.

The occurrence of wind erosion depends on the erosivity (i.e., wind speed) and the erodibility (i.e., land surface conditions). The vital land surface conditions in the Mongolian dust source area are the amount and distribution of vegetation and soil moisture. In addition, soil freeze–thaw processes and snow cover should be taken into consideration as the erodibility factors in this high-latitude area. Despite the importance of this dust source hotspot in East Asia, very little observation has been done on the complex processes of how those land surface conditions seasonally affect wind erosion in and around the hotspot. In turn, wind erosion is a major abiotic mechanism for moving material and thus responsible for cascading land-degradation phenomena in drylands. When topsoil is eroded by wind, the soil properties (e.g., soil texture, nutrients and organic material) are changed and redistributed, and thus affect the amount and distribution of vegetation. However, there is a lack of knowledge on the effects of wind erosion on ecosystem dynamics.

In this study, we used a process-based ecosystem (DAYCENT) model and field observation dataset (e.g., weather, saltation and vegetation) to investigate (1) the impacts of land surface conditions on wind erosion, and (2) the potential impacts of wind erosion on ecosystem dynamics, in a dust source hotspot of Mongolia (Tsogt-Ovoo in the desert steppe) in the 2000s.

In the first part, we integrated a unique 6-year measurement of saltation and simulated land surface elements (vegetation components of litter, live, and standing dead and soil temperature and moisture) by the DAYCENT ecosystem model, to investigate the effects of land surface conditions on wind erosion at Tsogt-Ovoo (TsO) in the desert steppe during 2012–2017. Saltation tended to occur during February–June with strong westerly winds (>10 m s^{-1}) and the highest frequencies in 2012 and 2015. The saltation season was divided into two periods based on seasonal variations in threshold wind speed for saltation (U_t): spring (February–early May) with an increase in saltation (i.e., a decrease in U_t); and early summer (late May–July) with a decrease in saltation (i.e., an increase in U_t). Multiple regression analysis revealed that for 2012 and 2015, U_t was negatively correlated with soil surface temperature in spring and positively correlated with vegetation components of live and standing dead in early summer. These correlations suggest that saltation was enhanced through soil freeze–thaw processes in spring and suppressed during early summer through plant growth in addition to dead leaves that are residues from the preceding summer. We propose a novel predictive tool to explain the temporal changes in U_t during the saltation seasons of 2012–2017. The results show that frequent saltation in 2012 and 2015 resulted from a combination of frequent strong winds and a low U_t, which was related to changes in soil temperature and low standing dead and live grasses.

In the second part, to explore the potential impacts of wind erosion on ecosystem dynamics, we assumed a scenario of topsoil (0–0.1 m depth) for simulation: a potentially wind-eroded coarse-textured topsoil (the wind-eroded scenario), which comprised 1% clay and 99% sand. This scenario represents an extremely wind-eroded topsoil that had permanently lost the fine particles and gained sand particles due to wind erosion. We then

used the DAYCENT model to simulate vegetation dynamics and how much of the changes in plant production were attributable to environmental factors (water, nitrogen, and temperature). Finally, we compared the simulations of the wind-eroded scenario and the actual condition in two Mongolian grasslands (desert steppe and steppe). Generally, stresses owing to a lack of water and nitrogen had the most influence on plant production in the wind-eroded scenario. For the wind-eroded topsoil, plant production decreased with increasing water stress in the desert steppe. However, it slightly increased in the steppe because of an inverse texture effect, where water infiltrated from the coarse topsoil to the deeper root-zone due to lower soil evapotranspiration and thus facilitated vegetation growth. At that time, nitrogen supply became the primary factor limiting plant growth.

In conclusion, we highlight that it is important that vegetation components of live and standing dead and soil freeze–thaw processes affect wind erosion in the dust source hotspot in East Asia. Moreover, we deduce that water stress, which is caused by the wind-eroded topsoil, significantly affects plant production in the Mongolia grasslands, when compared with temperature and nitrogen stresses. This outcome is expected to contribute to improving the accuracy of dust emission model and designing effective land use management to control wind erosion in the Mongolian grasslands. This study provides new insights into the complex interactions between wind erosion and ecosystem dynamics.

論文要旨

風食は、世界の乾燥および半乾燥地域における重要な環境現象である。それは、発生源と風下の地域において、人間と家畜の健康状態や経済活動だけでなく、生態系プロセスにも大きな影響を及ぼしている。2000 年代以降、東アジアではダストイベントの数が増加しており、特に、モンゴル草原は、東アジアで最も頻繁にダストが発生するホットスポットのひとつとなっている。

風食の発生は、侵食能（erosivity、風食を引き起こす風の能力）と受食性（erodibility、風食に対する土壌・地表面の侵食のされやすさ）の 2 つに依存する。侵食能は風速のみで表現できるのに対して、受食性は様々な地表面要素に関係する。モンゴルのダスト発生源における重要な地表面要素は、植生の量とパターン、土壌水分である。さらに、高緯度地域にあるモンゴルでは、土壌の凍結・融解プロセスおよび積雪も考慮に入れる必要がある。しかしながら、これらの地表面状態が風食にどのように影響するかという複雑なプロセスについては、いまだに十分に解明されていない。逆に、風食は物質を移動させる主要な非生物的メカニズムであり、乾燥地における土地劣化現象の原因となる。表土が強風によって侵食されると、土壌の特性（土性、栄養素、有機物など）が変化して再分配されるため、植生の量とパターンに影響を与える。しかしながら、風食がこれらの生態系プロセスに与える影響についての知識は不足している。

本研究では、生態系プロセスモデル（DAYCENT）と観測データセット（気候、saltation、植生量など）を使用して、2000 年代におけるモンゴルのダスト発生ホットスポットにおいて、(1) 地表面状態が風食に与える影響および (2) 風食が生態系プロセスに及ぼす潜在的な影響を調査した。

まず、現地観測による 6 年間（2012 年～2017 年）の saltation データと DAYCENT 生態系モデルによりシミュレートされた地表面要素を統合し、ゴビ

砂漠ステップにあるTsogt-0voo（Ts0）において、風食に対する地表面要素（土壌水分・温度、植生成分の生存体・枯死体・リター）の影響を調べた。Ts0での風食は、強い偏西風（> 10 m s^{-1}）により2月から6月にかけて発生する傾向があり、2012年および2015年に最も頻繁に風食が観測された。土壌粒子が舞い上がり始める風速（臨界風速、U_t）に基づいて、風食の季節は、saltationが増加する（U_tが減少する）春（2月から5月上旬）およびsaltationが減少する（U_tが増加する）初夏（5月下旬から7月）の2つの期間に分けられた。重回帰分析により、2012 年および 2015 年には、U_tは春の土壌表面温度および初夏の生存体・枯死体と、有意な相関があった。これらの相関関係から、土壌凍結・融解プロセスによって春の風食が強化され、前年夏の残留物である枯草に加えて初夏に成長する植物によって、風食が抑制されたことが示唆された。さらに、U_tの時間変化を説明するための、新しい予測ツールを提案した。その結果、2012 年および2015年の風食は、頻発した強風および低いU_t（土壌表面温度および枯死体・生存体）の組み合わせに起因することが示された。

次に、風食が生態系プロセスに与える潜在的な影響を調査するため、極端な風食のシナリオ（風食シナリオ）を想定した。このシナリオには、表土（深度0〜0.1m）が1%の粘土と99%の砂で構成されている。これは、風食によって粘土の大半失われ、それが砂に入れ替わった表土を表している。DAYCENTモデルを使用して、植生のダイナミクスをシミュレートすることによって、環境要因（水、窒素、温度）がどの程度、植物生産の変化をもたらすかを推定し、2つのモンゴル草原（ゴビ砂漠ステップとステップ）において、風食シナリオのシミュレーションと実際の状態を比較した。一般的に、水と窒素の不足によるストレスは、風食シナリオで植物生産量の減少により大きな影響を及ぼすと考えられている。風食された表土では、ゴビ砂漠ステップにおいて水ストレスの増加に伴い、

植物生産量が大きく減少したが、逆土性効果（inverse texture effect）により、ステップでは植物生産量がわずかに増加した。逆土性効果とは、水が粗い表土からより深い根圏に浸透し、土壌表面の蒸発散量が少ないために、植生の成長を促進することである。

本研究では、モンゴルのダスト発生ホットスポットにおける、生存体・枯死体および土壌凍結・融解プロセスが風食に大きな影響を与えていることを明らかにした。さらに、風食された表土によって引き起こされる水ストレスは、温度および窒素ストレスと比較して、植物生産量により大きな影響を与えることを明らかにした。この結果は、ダスト発生モデルの精度向上や風食を抑制するための有効な土地管理の設計に貢献することが期待できる。これにより、生態系ダイナミクスと風食の間の複雑な相互作用への新しい洞察を提供することができた。

Contents

1. Introduction

Soil erosion by wind is an important environmental phenomenon in arid and semi-arid regions worldwide. On a global scale, 11.2% of these areas are affected by wind erosion, with 35% of them in Asia (Middleton and Thomas, 1997). It has substantial influences on human and livestock health conditions, economic activities, and ecosystem dynamics, in both the source and downwind areas. Moreover, over recent decades, aeolian erosion has become increasingly severe globally, including those on temperate grasslands (Shinoda et al., 2011). Particularly, the Mongolian grasslands are a dust source hotspot with the highest frequencies dust outbreak in East Asia and an increasing number of dust events since the 2000s (Kurosaki et al., 2011b). Indeed, this region is recognized as one of the most vulnerable terrestrial ecosystems to wind erosion under climate change and human activity (Kassas, 1995; Lal, 2003; Shinoda et al., 2011).

The occurrence of wind erosion depends on the erosivity (i.e., wind speed) and the erodibility (i.e., land surface conditions) (United Nations Environment Programme, 1997). The threshold wind speed for saltation (U_t), which describes the initiation of mobilization of surface soil particles into the atmosphere, has been identified as an erodibility index (Ishizuka et al., 2009; Kurosaki et al., 2011b). Therefore, the discussion of wind erosion occurrence can be simplified into two aspects, wind speed and U_t. When wind speed overcomes U_t, wind erosion occurs. However, unlike wind speed, U_t is difficult to observe precisely in the field. This is because U_t is simultaneously affected by spatial and temporal soil and land surface characteristics, such as soil particle size distribution, soil moisture, soil crust, soil freeze–thaw processes, vegetation, snow cover, and land use (e.g., Bilbro and Fryrear, 1994; Fécan et al., 1998; Hoffmann et al., 2008; Ishizuka et al., 2005, 2009; Kim and Choi, 2015; Kurosaki et al., 2004, 2011a, 2011b; Nandintsetseg and

Shinoda, 2015; Shao, 2001).

In the dust source hotspot in East Asia, the amount and distribution of vegetation play an important role in controlling wind erosion (Shinoda et al., 2011). Vegetation is predominantly grass that cycles through a growth pattern, which at different times of the year can include prostrate plants (litter), senescent plants (standing dead grasses), and live plants, that protect the surface differently and with different efficiencies (Bilbro and Fryrear, 1994; Field et al., 2010; Nandintsetseg and Shinoda, 2015; Shinoda et al., 2011;). Consequently, the relationships between wind erosion and different vegetation components are investigated. Kurosaki et al. (2011a, 2011b) and Nandintsetseg and Shinoda (2015) proposed that higher levels of dead vegetation in spring, which are residues of vegetation from the preceding summer, can increase U_{t} and reduce wind erosion occurrence. Satellite-based remote sensing observation showed that vegetation growth from spring is the main controlling factor of U_{t} and significantly suppresses dust emission in the summer (Kurosaki and Mikami, 2007; Sugimoto et al., 2010). Furthermore, previous studies hypothesized that soil freeze–thaw processes in spring possibly cause changes in soil surface structure (e.g., Pawluk, 1988; Kværnø and Øygarden, 2006; Wei et al., 2019), which can lead to a decrease in U_{t} and thus affect the frequency and magnitude of wind erosion (Abulaiti et al., 2014). Variations in surface soil moisture by snow melting and ephemeral rainfall critically affect the threshold for wind erosion in East Asia (e.g., Ishizuka et al., 2005, 2009; Li and Zhang, 2014; Kim and Choi, 2015; Nandintsetseg and Shinoda, 2015; Yang et al., 2019). A study showed that snow cover in spring should be taken into consideration as an erodibility factor in this high-latitude area (Kurosaki and Mikami, 2004). Although a several of experimental studies have investigated the relationships between land surface conditions and wind erosion in

the steppe (e.g., Shinoda et al., 2010; Nandintsetseg and Shinoda, 2015), very little observation has been done on the complex processes of how those land surface conditions seasonally affect wind erosion in the dust source hotspot in the desert steppe.

In turn, wind erosion is a major abiotic mechanism for moving material, and thus responsible for cascading land-degradation phenomena in drylands (Breshear et al., 2003; Ravi et al., 2011). It affects ecosystem at different scales and contributes important biophysical feedbacks between biotic and abiotic components of Earth systems (Ravi et al., 2011; Shao et al., 2011), particularly the interactions between wind erosion and ecosystem dynamics. During wind erosion, fine particles (< 125 μm) are permanently removed from the parent soil surface and redistributed elsewhere by aerodynamic lift, saltation bombardment, and disaggregation (Shao, 2008). At the same time, the texture of the topsoil becomes increasingly coarse (Li et al., 2009; Yan et al., 2018) because of the accumulation of large amounts of sand-sized particles that hop along with the topsoil by saltation (Shao, 2008) from the windward side. Consequently, when topsoil is eroded by wind, the soil properties (e.g., soil texture, nutrients and organic material) are changed and redistributed, and thus affect the amount and distribution of vegetation.

Plant growth is generally affected by environmental factors, including temperature, light, water, and nutrients. These environmental factors deviating from the optimal intensity or quantity for the plant are called stress factors (Schulze et al., 2005). Water is the factor that most limits plant productivity. Studies have shown that growth rates are proportional to water availability when the temperature is suitable for plant growth in arid and semi-arid regions (Noy-Meir, 1973). Furthermore, productivity may be limited under temperature extremes and low soil nutrient contents (Szymańska et al., 2017). The coarser eroded soil in the top layer has less ability to retain water because of a decrease in the

water-holding capacity (Saxton and Rawls, 2006; Zhao et al., 2006) and an increase in the saturated hydraulic conductivity of the soil (Yao et al., 2013). This indicates that the water supply to the plant may be limited, causing an increase in water stress and a decrease in plant production (Yin et al., 2019). Conversely, previous studies reported that there is more evaporation from fine-textured than from coarse-textured soils in arid and semi-arid regions (Alizai and Hulbert, 1970; Noy-Meir, 1973). This effect may effectively trigger competition for moisture in the root-zone and lead to a decrease in the impact of water stress on plant production (Noy-Meir, 1973). Besides, some field studies and simulations have shown that wind erosion plays a vital role in the depletion and redistribution of soil organic carbon (SOC) and a variety of soil nutrients (Li et al., 2004; Li et al., 2008). When SOC and nutrients (e.g., nitrogen, N) are irreversibly removed by wind erosion, the productivity or fertility of the parent soil declines (Lal et al., 2001; Ravi et al., 2010), and the demand for nutrients stress from plant production increases (LeBauer and Treseder, 2008). However, there is a lack of knowledge on the effects of wind erosion on ecosystem dynamics in the dust source hotspot in East Asia.

A few models have simulated the interactions between wind erosion and ecosystem dynamics, including the Vegetation and Sediment Transport (ViSTA) model (Mayaud et al., 2017) and the ecological-wind erosion (ECO-WEMO) model (Zhang, 2020). However, previous studies neglected the effects of plant life cycle on wind erosion (Shinoda et al., 2011). Moreover, the effects of the coarsening of topsails by wind erosion on the cycles of water, carbon (C) and nutrients (e.g., N) should be taken into consideration (Zhao et al., 2006; Li et al., 2009). Therefore, to solve these gaps, in this study, we used an ecosystem-level biogeochemical model (DAYCENT) and field observation dataset (e.g., weather, saltation and vegetation), to investigate: (objective 1)

the impacts of land surface conditions on wind erosion, and (objective 2) the potential impacts of wind erosion on ecosystem dynamics, in the dust source hotspot in East Asia in the 2000s (Figure 1.1). The DAYCENT model simulates how fluxes of water, C, and nutrients (e.g., N) in the atmosphere, soil, and plants change in response to human activity. This model has been used to assess global grassland ecosystem dynamics under different land-use conditions (e.g., grazing) and climate change impacts.

In 2012, a new site for advanced dust monitoring was initiated at Tsogt-Ovoo (TsO), which is located on the northern Gobi Desert of Mongolia, and is a hotspot of dust outbreak in East Asia (Natsagdorj et al., 2003; Kurosaki and Miami, 2007; Kurosaki et al., 2011a; Ishizuka et al., 2012; Abulaiti et al., 2014). For the first objective, we integrated a unique 6-year measurement of saltation and simulated land surface elements (vegetation components of litter, live, and standing dead and soil temperature and moisture) by the DAYCENT ecosystem model, to investigate the effects of land surface conditions on wind erosion at TsO during 2012–2017. Possible land surface parameters that suppress saltation were simulated and validated with long-term observations. We then calculated U_t based on measurements of saltation number and wind speed. Finally, these simulated land surface variables were used to identify the best models for U_t during saltation season by correlation and multiple regression analysis.

For the second objective, to explore the potential impacts of wind erosion on ecosystem dynamics, we specified an assumed scenario of topsoil (0–0.1m depth) for simulation: a potentially wind-eroded coarse-textured topsoil (the wind-eroded scenario), which comprised 1% clay and 99% sand. This scenario represents an extremely wind-eroded topsoil that had permanently lost the fine particles and gained sand particles due to wind erosion. We then used the DAYCENT model to simulate vegetation dynamics

and how much of the changes in plant production were attributable to environmental factors (water, nitrogen and temperature). Finally, we compared the simulations of the wind-eroded scenario and the actual condition in two Mongolian grasslands (desert steppe and steppe).

2. Methods and Materials

2.1. Site description and land surface measurement

The two study sites are in the Mongolian grasslands (Figure 2.1). One site, Bayan-Unjuul (BU: 47.04˚N, 105.95˚E), is on the steppe and has a semi-arid climate, while the other, Tsogt-Ovoo (TsO: 44.42˚N, 105.39˚E), is on the desert steppe and has an arid climate. These two sites are in the north (BU) and the middle (TsO) of the dust source area. To gain insights into the relationships between dust emissions and ecosystem dynamics (e.g., vegetation, soil moisture, and land use), the Dust-Vegetation Interaction Experiment (DUVEX) at BU (refer as BU site), which has an area of 50 m × 35 m, was established in 2007 on vegetated land surfaces (Nandintsetseg and Shinoda, 2015; Shinoda et al., 2010). Kurosaki et al. (2011), Nandintsetseg and Shinoda (2015) and Shinoda et al. (2011) suggested that vegetation growth-decay cycle is critical for wind erosion in temperate grasslands. Previous studies figured out the highest frequency of dust emission in East Asia occurred at TsO based on meteorological observatory data (Kurosaki and Mikami, 2007; Abulaiti et al., 2014; Qi et al., 2018). Since 2012, the DUVEX project was therefore extended to include a trapezoidal dust observation site at TsO (refer as TsO site) with 40 m on the log side, 20 m on the short side, and 28 m in height (Ishizuka et al., 2012).

Meteorological data were obtained from the Mongolian Institute of Meteorology, Hydrology, and the Environment (IRIMHE) from 2002–2011 at BU and 2002–2017 at TsO. The average annual precipitation amounted to 145.1 mm with 116.9 mm during the growing season (May–September) at BU, and 85.3 mm with 71.5 mm during the growing season at TsO, respectively. The annual mean temperature was 0.86°C at BU and 5.1°C at TsO, respectively.

The Mongolian grasslands are typically dominated by the C3 vegetation type (Nandintsetseg and Shinoda, 2015). At BU, small shrubs (*Caragana spp.*), perennial grasses (*Cleistogenes squarrosa*, *Stipa grandis*, and *Stipa krylovii*) and forbs (*Artemissia spp.*), and dominate, while desert shrubs (*Reaumuria soongolica* and *Salsola passerine*) dominate at TsO (Hilbig, 1995; Ishizuka et al., 2012). The aboveground vegetation mass (standing dead and live grasses, AGM) in the grazing areas at BU site was measured approximately monthly in June, July, and August (mostly August) from 2003 to 2010 (Nandintsetseg and Shinoda, 2015). Measurements of AGM (2002–2015) in the grazing area at TsO IRIMHE monitoring station were also obtained. These AGM samples were conducted by clipping all plants within four 1 m × 1 m quadrants in the grazing area. The vegetation covers in the peak season (at the end of August) of the steppe (BU) during 2004–2019 and the desert steppe (TsO) during 2012–2018 were 55% and 20%, respectively. The grazing intensity at BU and TsO sites was identified as light grazing (Sugita et al., 2007) and heavy grazing, respectively.

Soils at BU and TsO sites are mostly Kastanozems and Kastanozem calcic skeletic (Kinugasa et al., 2012; Dordjgotov, 2003). The soil texture in the topsoil (0–0.1 m depth) is 65% sand and 9% clay at BU site, and 64% sand and 17% clay at TsO site, respectively. Average soil C and total nitrogen at BU site (0.1 m depth) in August during 2004–2008 were 6.42 g kg^{-1} and 0.71 g kg^{-1} (Shinoda et al., 2010), respectively. Soil C and NO_3^- at TsO site (0.1 m depth) in August 2017 were 3.63 g kg^{-1} and 5.13 ppm, respectively.

The volumetric soil moisture content (%) was observed hourly at depths of 0.1 m at BU site (2004–2008) (Nandintsetseg and Shinoda, 2015; Shinoda et al., 2010), and of 0.1 and 0.025 m at TsO site (2012–2015) (Ishizuka et al., 2012) using time-domain reflectometry (Delta-T; ML2x). At TsO site, we also measured soil maximum and

minimum temperature ($SoilT_{\max}$ and $SoilT_{\min}$) at 0.025 m depth with a platinum resistance thermometer (C-PTG-10) during 2012–2015, wind speed (m s^{-1}) and direction with R.M. Young; YG-5103 sensor at 3 m height during 2012–2017, and saltation number (count per minute) with a piezoelectric sensor during 2012– 017 (Sensit Co., Portland, ND, USA) at 0.059 m height.

2.2. Estimation of threshold wind speed for saltation (U_t)

For the first objective of the study, we estimated the threshold wind speed for saltation (U_t). U_t was determined using the measured saltation number by piezoelectric sensors based on the least square's technique and the Nash-Sutcliffe model efficiency coefficient (NSE) (Nash and Sutcliffe, 1970).

First, we determined U_t using the following equation (Eq. 1, Shinoda et al., 2010; Abulaiti et al., 2014), which is similar to that proposed for threshold friction velocity by Owen (1964), Shao and Mikami (2005), and Ishizuka et al. (2009). The squared difference e of saltation number between observed and modelled data was calculated for each minute:

$$SN_{\mathrm{mod}} = \begin{cases} 0, & U < U_t \\ C\left(1 - \frac{{U_t}^2}{U^2}\right)U^3, & U > U_t \end{cases} \quad (1)$$

$$e = (SN_{\mathrm{obs}} - SN_{\mathrm{mod}})^2 \quad (2)$$

where SN_{obs} and SN_{mod} are the saltation number per minute at a reference height obtained by piezoelectric sensor and modelling, respectively. C is an empirical coefficient (g s^2 m^{-5}) that is dependent on sand particle size, and U is wind speed (m s^{-1}) at 3 m height.

Second, e was summed as E within one day for a certain U_t and C:

$$E = \sum e\,(U_t, C) \quad (3)$$

Third, E was calculated by changing both U_t and C increments of 0.01 m s^{-1} and 0.01 g s^2 m^{-5}, respectively, based on Ishizuka et al. (2009). The saltation number was the same for every E calculation even when U was smaller than U_t.

Finally, when achieved a minimum value within one day, the values of daily U_t and C were determined. Moreover, to evaluate the overall predictive power of each model per day, the normalized goodness-of-fit statistics were calculated. The Nash-Sutcliffe model efficiency coefficient (NSE) was therefore used in this study (Sterk et al., 2012; Pi and Sharratt, 2019):

$$NSE = 1 - \frac{\sum(SN_{obs} - SN_{mod})^2}{\sum(SN_{obs} - \overline{SN_{obs}})} \quad (4)$$

where $\overline{SN_{obs}}$ is the average of the observed total saltation number per minute in one day. Values of NSE can range from –∞ to 1. The more accurate the model, the closer the model efficiency is to 1. Values between 0 and 1 are generally viewed as acceptable levels of model performance, however, the mean observed value is a better predictor than the modelled value if $NSE \leq 0$. Previous studies have defined the threshold value for acceptable model efficiency when $NSE \geq 0.50$ (Moriasi et al., 2007; Ritter and Munoz-Carpena, 2013).

2.3. Statistical analysis of relationships between land surface elements and U_t

To clarify the appropriate explanatory variables in U_t, we applied stepwise multiple regression analysis for two saltation periods using data (12 days for spring and 20 days for early summer) from the two strongest saltation years (2012 and 2015). We considered up to six possible predictive variables to explain the temporal variations of U_t (as the dependent variable). These six variables are daily surface soil moisture, 10-day moving

averaged $SoilT_{\max}$ and $SoilT_{\min}$ ($SoilT_{\text{10-day-max}}$ and $SoilT_{\text{10-day-min}}$), vegetation components of litter, live, and standing dead. First, to identify the factor that most influenced U_t, correlation analyses were carried out using U_t and each individual variable. Then, stepwise multiple regression was run using U_t and its significantly related surface variables for each period. The best models for each period were chosen using the criteria of the best fit of significant variables to the data. To investigate the effects of sequential soil freeze–thaw processes on U_t, we used $SoilT_{\text{10-day-max}}$ and $SoilT_{\text{10-day-min}}$.

2.4. Description of the DAYCENT ecosystem model

For the first and second objective of the study, we used the DAYCENT model to simulate the land-surface elements at TsO and BU sites in the Mongolian grasslands. The DAYCENT model, which is the daily time-step version of the CENTURY biogeochemical model (Parton et al., 1993), is a process-based terrestrial ecosystem model that simulates how fluxes of water, C, nutrients (e.g., N, phosphorus, and sulfur) in the plant, soil, and atmosphere, change in response to human activity (e.g., fire and grazing) (Del Grosso et al., 2001; Parton et al., 1998). The model input parameters include (1) climatic parameters (daily air maximum and minimum temperatures and precipitation), (2) site-specific parameters such as soil properties (texture, bulk density, field capacity, depths of soil layers, and pH) (Table 2.1), and (3) land management (e.g., cultivation or grazing). This model includes submodels of soil water and temperature dynamics, decomposition of soil organic matter (SOM) and dead plant material, nitrogen gas fluxes, and plant productivity (Figure 2.2).

The plant production submodel (Parton et al., 1993) can simulate a variety of

ecosystems, including grasslands (Gilmanov et al., 1997; Nandintsetseg and Shinoda., 2015), by altering various plant-specific parameters so that different herbaceous crops (corn, wheat, etc.) and plant communities (C3, C4, etc.) are represented. This submodel is related to soil nutrients and organic cycling submodels and considers plant productivity as a function of genetic potential, phenology, nutrient availability, water/temperature stress, and solar radiation. Biomass can be removed or transferred to the litter pool by disturbances such as grazing. Grazing effects on vegetation are identified by Holland et al. (1992) and Ojima and Correll (2009).

The land surface submodel simulates the soil surface moisture and temperature dynamics. This submodel simulates the soil water flow through litter, the plant canopy, and soil layers (0–2 cm, 2–5 cm, 5–10 cm, 10–15 cm, 15–30cm, and others) and has been tested extensively (Parton et al., 1998; Nandintsetseg and Shinoda, 2015). The amount of water in the soil that is available for plant growth is calculated by precipitation, the current soil water, and potential evapotranspiration (PET) (Parton et al., 1998). Intercepted precipitation by vegetation is evaporated at the PET rate. This rate is estimated by Penman (1948). The amount of water intercepted is a function of the plant biomass and rainfall amount (Parton et al., 1998). When the daily air temperature is below freezing, precipitation is assumed to fall as snow and is accumulated in the snowpack. The daily soil minimum and maximum temperatures at soil depths of 0–2, 2–5, 5–10, 10–20 cm, and others, are simulated by the one-dimensional Fourier heat transfer equation (Munn, 1966; Parton 1984). The diurnal temperature range at the soil surface is dependent on the snow water equivalent above the soil surface and daily air maximum and minimum temperatures measured at 2 m above the soil surface (Parton et al., 1984, 1998).

The SOM submodel simulates the dynamics of C and N in the organic and inorganic

parts of the soil system that represent the flow of C, N in plant litter, and different organic and inorganic soil pools, with mineralization of soil nutrients primarily resulting from the turnover of soil organic matter pools. The N submodel, which has the same structure as the soil C submodel (Parton et al., 1993, 1998; Del Grosso et al., 2001), was the focus of this study. The N flows follow the C flows and are equal to the product of the C flows and the C:N ratio of the state variable that receives the C. The inputs of N can be calculated using equations for atmospheric deposition and soil and plant N fixation. The N losses due to leaching are related to the soil texture and the amount of water moving through the soil profile (Parton et al., 1998).

2.5. Model parameterization

We used the daily meteorological (maximum and minimum air temperatures and precipitation) data from the IRIMHE monitoring stations at BU (1980–2011) and TsO (1980–2017) as model inputs. The field-measured data were used for the DAYCENT model validations and simulations. Previous studies have shown that global grassland ecosystems can be simulated using relatively few site-specific parameters that change as the circumstances change (Parton et al., 1993). The DAYCENT model was parameterized and calibrated with the field experiment data (vegetation and soil chemical and physical properties) at BU site (Nandintsetseg and Shinoda, 2015) and TsO site (Table 2.1). The maximum potential (or genetic maximum) aboveground plant production ($AGP_{\max}$) and the maximum and optimum temperatures for plant production were parameterized using information from the Mongolian grasslands' agrometeorological database (IMH, 1996).

The soil and vegetation were in equilibrium for the actual condition and the wind-eroded scenario at BU and TsO sites, historical simulations were processed in the

DAYCENT model for 1980 years by repeating the long-term climate averages over 32 years (1980–2011) for BU site and 38 years (1980–2017) for TsO site. The actual daily meteorological data sets were then used to run the real grazing conditions (light grazing for BU site from 1980 to 2011 and heavy grazing for TsO site from 1980 to 2017). The model performance is assessed from the mean absolute deviation (D_{abs}), and the Pearson correlation coefficient (r), slope and intercept coefficient from the linear regression equation of the observations versus the corresponding simulations (Gilmanov et al., 1997; Nandintsetseg and Shinoda, 2015).

2.6. Simulations for the actual condition and the wind-eroded scenario

The simulations aimed to examine how plant productivity changes in the wind-eroded coarse-textured topsoil in the Mongolian grasslands. Relatively few studies have discussed that vegetation changes because of changes in soil texture driven by wind erosion as they occur slowly (Larney et al., 1998) and may become noticeable after several years or decades. In this study, we compared plant production simulations in two different conditions of soil texture in topsoil. We assumed a wind-eroded scenario that topsoil was seriously eroded by wind. For this scenario, a topsoil (0–0.1 m depth) that comprised 1% clay, 0% silt, and 99% sand was used. Lyles and Tatarko (1986) reported that the topsoil's sand content increased with a range from 0.9 to 23.3%, and 7.2% of silt content was removed through sorting by wind over 36 years in the central and southern Great Plains. Li et al. (2009) showed that two years of wind-erosion has resulted in a reduction in fine particles (by 1.5%) and an increment in sand particles (by 2.7%) in topsoil. Therefore, our wind-eroded assumption represents topsoil in severe wind erosion areas that soil had permanently lost most of the fine particles from its surface by dust

emissions due to aerodynamic entrainment, saltation bombardment, and aggregate disintegration, and left coarse particles that supplemented through saltation (Shao, 2008) from the windward side. On the other hand, an actual field condition was used to simulate based on the observed data of the topsoil texture.

2.7. Simulating of water, temperature, and nitrogen stresses with the DAYCENT model

In the DAYCENT grassland submodel, plant production is controlled by initially having soil moisture and temperature at a maximum and then decreased if the soil nutrient supply is insufficient. This submodel includes the effect of shading from dead vegetation on plant production (Parton et al., 1993). During the simulation processes, $AGP_{\max}$, not limited by temperature, water, or nutrient stresses, is primarily determined by the level of photosynthetically active radiation, the maximum net assimilation rate of photosynthesis, the efficiency at which carbohydrates are converted into plant constituents, and the rate at which respiration is maintained (Parton et al., 1993, 1998). Thus, the parameter for $AGP_{\max}$ has both genetic and environmental components. The potential production (AGP_{pot}) is a function of $AGP_{\max}$ for grassland and the 0–1 environmental scalars depending on soil temperature, soil water status, shading from dead vegetation, and seedling growth (Parton et al., 1993). Here, seedling growth and shading from dead vegetation have a negligible effect on AGP_{pot}, because the seedling growth for grass is not limited (Parton et al., 1992). And, the shading effect on AGP_{pot} is a response surface that depends on the amount of live and dead vegetation. We found that amounts of observed aboveground live and dead vegetation in the Mongolian grasslands were lower than the threshold values at which shading occurs and shoot senescence increases (150 and 60 g m^{-2}, respectively) (Parton et al., 1992). Therefore, we assumed that the soil water

status and temperature were the main controls on the AGP_{pot} in the Mongolian grasslands (Eq. 5). The effects of soil water availability and temperature on plant production (Water stress, W_{stress}; Temperature stress, T_{stress}) were calculated as shown in Eq. (6) and Eq. (7).

$$AGP_{\mathrm{pot}} = AGP_{\mathrm{max}} \times S_{\mathrm{T}} \times S_{\mathrm{w}} \quad (5)$$

$$T_{\mathrm{stress}} = 1 - S_{\mathrm{T}} \quad (6)$$

$$W_{\mathrm{stress}} = 1 - S_{\mathrm{w}} = 1 - \frac{AGP_{\mathrm{pot}}}{AGP_{\mathrm{max}} \times S_{\mathrm{T}}} \quad (7)$$

where S_{T} is an environmental scalar of soil temperature, which is calculated as a function of air temperature and the optimum plant temperature. S_{w} is an environmental scalar of soil moisture statue, which is identified by the soil-water sub-model (Parton et al., 1993). The values of T_{stress} and W_{stress} are both ranges from 0 to 1, and the values close to 1 indicate the maximum stress on plant production.

The plant production also decreases if there is an insufficient nutrient (e.g., N) for uptake and to satisfy the C: N ratio for producing plants. The actual production (AGP_{act}) is limited to what can be achieved with the nutrient supply available at the time with plant nutrient concentrations (Eq. 8). We assumed how the AGP_{act} was affected by the lack of N (nitrogen stress, N_{stress}) as shown in Eq. (9).

$$AGP_{\mathrm{act}} = AGP_{\mathrm{pot}} \times S_{\mathrm{N}} \quad (8)$$

$$N_{\mathrm{stress}} = 1 - S_{\mathrm{N}} = 1 - \frac{AGP_{\mathrm{act}}}{AGP_{\mathrm{pot}}} \quad (9)$$

where S_{N} is an environmental scalar of nitrogen insufficiency, which is identified by the soil organic matter and nutrient sub-models.

In this study, we mainly focused on the changes in the effects of W_{stress} and N_{stress} on AGP_{act} for the actual condition and the wind-eroded scenario during the critical

growing season (June–August). Eq. (10), Eq. (11), and Eq. (12) were proposed to examine the wind-eroded coarse-textured topsoil impacts on AGP_{act}:

$$\Delta AGP_{\mathrm{act}} = (AGP_{\mathrm{act}})_{\mathrm{eroded}} - (AGP_{\mathrm{act}})_{\mathrm{actual}} \quad (10)$$

$$\Delta W_{\mathrm{stress}} = (W_{\mathrm{stress}})_{\mathrm{eroded}} - (W_{\mathrm{stress}})_{\mathrm{actual}} \quad (11)$$

$$\Delta N_{\mathrm{stress}} = (N_{\mathrm{stress}})_{\mathrm{eroded}} - (N_{\mathrm{stress}})_{\mathrm{actual}} \quad (12)$$

where $\Delta AGP_{\mathrm{act}}$, $\Delta W_{\mathrm{stress}}$, and $\Delta N_{\mathrm{stress}}$ are the differences in the actual plant production, water stress, and nitrogen stress between the actual condition and the wind-eroded scenario. The subscripts "actual" and "eroded" denote the actual condition and the wind-eroded scenario, respectively.

The changes in the plant production between the actual condition and wind-eroded scenario ($\Delta AGP_{\mathrm{act}}$) were examined. For example, when $\Delta AGP_{\mathrm{act}} < 0$, AGP_{act} in the actual condition is higher than in the wind-eroded scenario. The reasons for the changes in $\Delta AGP_{\mathrm{act}}$ from $\Delta W_{\mathrm{stress}}$ and $\Delta N_{\mathrm{stress}}$ were also analyzed. When $\Delta W_{\mathrm{stress}} > 0$ and $\Delta N_{\mathrm{stress}} \leq 0$, plant production is mainly limited by water, while when $\Delta W_{\mathrm{stress}} < 0$ and $\Delta N_{\mathrm{stress}} > 0$, plant growth is limited by nitrogen.

3. Results

Generally, in the Mongolian dust source area, meteorological observation showed that wind erosion was weak in January, enhanced in April, and suppressed in July (Kurosaki and Mikami, 2007). The frequency of strong wind was high in spring and low in winter and summer (Kurosaki and Mikami, 2005). Field observation showed that the soil is frozen during winter (October–March) and diurnal soil temperature fluctuates across the freezing point during March–April. Soil moisture significantly depends on the balance between precipitation and evapotranspiration when the air temperature was > 0 °C (Nandintsetseg and Shinoda, 2010). Plant emergence and senescence occur in late April and mid-September, respectively. In this section, the results of the field measurement of saltation and simulations in the dust source hotspot are shown.

3.1. Seasonal and interannual variations in saltation and U_t in the desert steppe

The seasonal and interannual variations in monthly total saltation number and averaged daily maximum wind speed (U_{max}) during 2012–2017 are shown in Figure 3.1–a. Seasonally, saltation tended to occur in months of spring and early summer (February to July) each year, with almost no occurrence of saltation in late summer and winter (August to the following February). Interannually, saltation had significant differences year to year, with the strongest years occurring in 2012 and 2015. It was clearly shown that saltation occurred when U_{max} exceeded a certain threshold value.

The frequency distributions of wind direction for four ranges (< 5, 5–10, 10–15, > 15 m s^{-1}) of U_{max} and for saltation number during the saltation season (February to July) in 2012–2017 are shown in Figures 3.1–b and 3.1–c. Strong U_{max} of > 10 m s^{-1} was from west to northeast (W to NE), whereas weak U_{max} of > 10 m s^{-1} was from east-northeast

to east (ENE to E). During saltation occurrence, U_{max} from west to west-northwest (W to WNW) was predominant. This indicates that saltation generally occurred with a strong westerly wind speed of > 10 m s^{-1} in this region.

The daily variations in total saltation number with the measurement-based U_t by Eq. (1) during the saltation season in 2012–2017 are shown in Figure 3.2. During these six years, a total of 787 days had a saltation number above 0. 48 days of those (23 days in 2012, 6 days in 2013, 1 day in 2014, 13 days in 2015 and 5 days in 2016) were satisfactorily predicted for U_t during February–July, whereas no U_t values were predicted in other months. Saltation number generally increased from February and reached a peak in early May. After a peak in late May, saltation number decreased until July. Meanwhile, U_t showed temporal variations during the saltation season with decreasing U_t during February to early May (r = 0.74, p < 0.05) from 18.5 to 12.3 m s^{-1} and increasing U_t (r = 0.54, p < 0.05) during late May to July from 7.2 to 19.5 m s^{-1}. Based on these results, the saltation season was divided into two periods: spring (February–early May) with an increase in saltation (i.e., a decrease in U_t); and early summer (late May–July) with a decrease in saltation (i.e., an increase in U_t).

3.2. Model performance

The daily variations observed and simulated AGM, soil temperature and moisture with precipitation from 2002–2017 at TsO in the desert steppe are shown in Figure 3.3. And, the daily variations in precipitation and observed and simulated AGM and soil moisture from 2002–2011 at BU in the steppe are shown in Figure 3.4. Table 3.1 shows that the model gave reasonably good simulations of the variations in AGM and soil moisture at both sites and soil temperature at TsO. Generally, the timings of spring growth

onset (May), summer peak (July–August), and decay (September) are shown at both sites. The model underestimated the peak production in the years when the measured production was high and following drought years (e.g., 2008 at both sites), perhaps reflecting changes in the plant species composition during those years (Nandintsetseg and Shinoda, 2015). These simulations of soil moisture and temperature show a similar seasonal pattern with a previous observational study in the Mongolian grasslands (Nandintsetseg and Shinoda, 2011). Therefore, these results suggest that the DAYCENT model can give reasonable simulations of seasonal and interannual changes in AGM, and soil moisture and temperature at TsO and BU in the Mongolian dust source area.

3.3. Relationships between land surface elements and U_t in the desert steppe

The daily variations in saltation, the measurement-based and predicted U_t, and $U_{\max}$ with surface soil moisture, precipitation, $SoilT_{\text{10-day-max}}$ and $SoilT_{\text{10-day-min}}$, vegetation components of live and standing dead, during the saltation season in 2012–2017 are shown in Figure 3.5. Figure 3.5 shows that strong saltation events occurred in spring and early summer of 2012 and 2015 following continuous long-lasting droughts (Figure 3.3). For these two years, soil moisture was stable and less than 8% before April because the soil was frozen ($SoilT_{\text{10-day-max}} < 0$). $SoilT_{\text{10-day-max}}$ and $SoilT_{\text{10-day-min}}$ rose and exceeded 0 in mid-March and late April, respectively. Subsequently, soil moisture was affected by rainfall, however, it immediately evaporated because of high potential evapotranspiration (Nandintsetseg and Shinoda, 2011). For vegetation components, there was less standing dead vegetation in spring, which in turn was the result of drought in the preceding years (2011 and 2014). Moreover, due to the lack of soil moisture (late rainy season), plant growth was delayed until June.

To clarify the major factors controlling U_t among land surface variables for two periods (spring and early summer), we applied correlations with six possible predictable surface variables for the strong saltation in 2012 and 2015 (Table 3.2). Considering all individual variables effects, for the spring period, U_t was significantly correlated with $SoilT_{\text{10-day-max}}$ (r = –0.60, p < 0.05) and $SoilT_{\text{10-day-min}}$ (r = –0.65, p < 0.005), while for the early summer period, U_t was significantly correlated with $SoilT_{\text{10-day-max}}$ (r = –0.44, p < 0.05), $SoilT_{\text{10-day-min}}$ (r = –0.49, p < 0.05), and vegetation components of standing dead (r = 0.82, p < 0.001) and live (r = 0.49, p < 0.01). Therefore, these significantly correlated variables were chosen for identification of the best fit models by multiple regression. The best regression models with the highest adjusted determination coefficient (R^2_{adjusted}) (Table 3.2) show that for the spring period, the best model for U_t was selected based on $SoilT_{\text{10-day-min}}$, which accounted for 39% of the decrease in U_t. For the early summer period, the best model for U_t included the combination of standing dead and live vegetation and explained 70% of the increase in U_t.

3.4. Effects of water, temperature, and nitrogen stresses on plant production in the desert steppe and steppe

Figure 3.6 shows the monthly precipitation and temperature and simulated AGP_{act}, W_{stress}, N_{stress}, and T_{stress} values for the actual condition and the wind-eroded scenario at TsO and BU in the growing season (May–September) during 2002–2011. The monthly average AGP_{act} for the wind-eroded scenario was generally lower than for the actual condition at both sites, but AGP_{act} for the wind-eroded scenario at BU during June–August was higher than for the actual condition with 5.0% (Table 3.3). Soil moisture had more effect on AGP_{act} than soil temperature and nitrogen, and W_{stress} for both

scenarios was higher at TsO and BU. N_{stress} played an essential role for AGP_{act} at BU, but plant production at TsO was not affected by nitrogen. Table 3.3 shows that N_{stress} at BU for the wind-eroded scenario was higher than for the actual condition, with 19.3%. Soil temperature had a negligible effect on AGP_{act} during June–August at both sites. These results show that W_{stress} and N_{stress} influenced plant production in the growing season in the Mongolian grasslands, while T_{stress} was only significant in the emergence (May) and senescence (September) periods.

Figure 3.7 shows the differences in AGP_{act}, W_{stress}, and N_{stress} between the actual condition and the wind-eroded scenario (ΔAGP_{act}, ΔW_{stress}, and ΔN_{stress}) in the critical growing season (June–August) from 2002 to 2011 (total 30 months). ΔAGP_{act} had mean values of 0.38 (+5.0%) at BU and –0.14 (–20.2%) gC m^{-2} at TsO, respectively. Table 3.4 shows that plant production at TsO was mainly controlled by water ($\Delta W_{stress} > 0$ and $\Delta N_{stress} \leq 0$) for 28 months when ΔAGP_{act} was less than 0. These results show that plant production almost decreased in the wind-eroded scenario at TsO and this decrease was caused by an increase in water stress (Figure 3.7–d1). At BU, when ΔAGP_{act} was less than 0, plant production was mainly controlled by water for seven months and by nitrogen ($\Delta W_{stress} \leq 0$ and $\Delta N_{stress} > 0$) for two months. When ΔAGP_{act} was greater than 0, plant production was primarily controlled by water for five months and nitrogen for 14 months. These results show that this higher plant production at BU was primarily caused by reducing water stress and plant growth was then controlled by nitrogen in the critical growing season (Figure 3.7–a2).

4. Discussion

In this study, we forced on the relationships between wind erosion and ecosystem dynamics (Figure 4.1). In this section, we discuss these two questions: (1) the impacts of land surface conditions on wind erosion, and (2) the potential impacts of wind erosion on ecosystem dynamics.

4.1. Seasonal and interannual variations in land surface conditions effects on wind erosion

In the first part of this study, we analyzed the possible land surface elements and the best model for U_t in the spring and early summer periods for 2012 and 2015 at TsO in the desert steppe (Table 3.2). For the spring period, the best model for U_t was selected based on $SoilT_{10\text{-day-min}}$. This implies that saltation in spring was likely enhanced through soil freeze–thaw processes (Kim, 2008; Abulaiti et al., 2014). Previous studies of laboratory experiments (Domby and Kohnke, 1955; Oztas and Fayetorbay, 2003; Kværnø and Øygarden, 2006; Žabenská and Dumbrovský, 2015; Wei et al., 2019) and hypothesis based on field observations (Abulaiti et al., 2014; Han et al., 2010, 2011) both reported that soil freeze–thaw processes play an important role in increasing dust outbreak and wind erosion because these processes can affect soil properties and change soil aggregate size distribution. Pawluk et al. (1988) observed that repeated freezing and thawing increases the number of coarse voids in soil but with a consequent marked reduction in the number of fine voids. Ferrick and Gatto (2005) determined that ice within soil voids forced particles apart and could compress or rupture soil aggregates during periods of the water freezing. Therefore, the successive freeze–thaw cycles under natural conditions increased the disruption of soil surface aggregates and was possibly related to the decrease

in U_t. In addition, the lower $R^2_{adjusted}$ in this period indicates that other erodibility factors affected wind erosion. Kurosaki and Mikami (2004) determined that the threshold for dust emission substantially decreases with reducing snow cover in spring, particularly in April. Lee and Kim (2012) clarified that dust outbreaks in the Gobi Desert region are relatively sensitive to snow cover. A crust, which is temporarily formed after a small amount of precipitation or snowmelt, causes a significant increase in U_t and affects wind erosion processes when soil moisture and vegetation cover are low and rarely changed in relatively dry areas (Ishizuka et al., 2008, 2012; Abulaiti et al., 2014).

For the early summer period, the best model for U_t included the combination of live and standing dead grasses. This shows that standing dead vegetation had a greater effect on U_t, indicating that it was a crucial factor in suppressing saltation during this period. Following other factors in spring, such as soil freeze–thaw processes, these dead leaves consequently control the soil erodibility (Kurosaki et al., 2011a). Previous studies revealed that dead leaves of vegetation in spring, which are the residual vegetation from the preceding summer, are the main factor suppressing dust events, the so-called "Dead-leaf hypothesis" (Kurosaki et al., 2011a, 2011b; Nandintsetseg and Shinoda, 2015; Shinoda et al., 2011). Therefore the dead-leaf hypothesis is verified in the results. Subsequently, U_t was affected by plant growth; live vegetation continued to increase until the end of July with increasing U_t, thereby suppressing wind erosion. Satellite-based studies reported that vegetation growth with slight precipitation in the Gobi Desert area significantly reduces dust emission (Sugimoto et al., 2010). Generally, vegetation reduces erodibility by reducing wind momentum, protecting surface cover, and catching particles, thereby increasing U_t, and significantly suppressing wind erosion. In addition, a previous study reported that litter is not significantly correlated with spring dust events

in this region because of its short memory (Nandintsetseg and Shinoda, 2015). These results of vegetation effects are consistent with those of previous studies (Bilbro and Fryrear, 1994; Shinoda et al., 2011). These studies have suggested that vegetation components of standing dead, live or litter protect the surface differently and with different efficiency.

For both periods, U_t was not significantly correlated with soil moisture (Table 3.2). Previous studies reported that soil moisture is an important factor influencing U_t in different wind-eroded areas (Fécan et al., 1998; Ishizuka et al., 2005, 2009; Kim and Choi, 2015; Nandintsetseg and Shinoda, 2015; Yang et al., 2019). It is because the seasonal and interannual precipitation can substantially affect soil moisture in relatively wet areas of the dryland (e.g., steppe area) (Nandintsetseg and Shinoda, 2013, 2015). Nevertheless, the effects of soil moisture are limited in the Gobi Desert with soil moisture ranging between 2–8% (Abulaiti and Kimura, 2011; Abulaiti et al., 2014; Li and Zhang, 2014) (Figure 3.5). This implies that a regional difference in land surface conditions, which corresponded to the temperature and precipitation gradients, control the occurrence of wind erosion.

Due to the significant difference in R^2_{adjusted} between these two periods, there was likely a transition from the spring to the early summer during the saltation season. These erratic changes were likely linked to the seasonal and interannual changes in climate and human activity. Seasonal and interannual changes in soil temperature, and thus in timing and duration of freeze–thaw cycles in the spring can help to moderate the destruction of soil texture (Lehrsch et al., 1991, 1998; Kværnø and Øygarden, 2006; Žabenská and Dumbrovský, 2015). Moreover, the effect of standing dead vegetation on wind erosion varies depending on previous summer precipitation and grazing intensity (Shinoda et al.,

2010; Kurosaki et al., 2011a; Nandintsetseg and Shinoda, 2015). Therefore, it is complicated to identify the timing and duration of this transition period. Here, we propose a novel predictive tool to explain the temporal changes in U_t during the saltation seasons of 2012–2017 with the best models of U_t for the two periods of 2012 and 2015 by selecting the maximum values of predicted U_t (Eq. 5):

$$U_t^{pre} = \max(f(\text{Spring}),\ f(\text{Early summer})) \quad (5)$$

U_t^{pre} is predicted U_t, and $f(\text{Spring})$ and $f(\text{Early summer})$ indicate the best models of U_t for the two periods of 2012 and 2015 (Table 3.2). U_t^{pre} is well-matched with the measurement-based U_t ($r = 0.97$, $p < 0.05$). Frequent saltation in 2012 and 2015 resulted from a combination of frequent strong winds and a low U_t, which was related to changes in soil temperature and low standing dead and live grasses (Figure 3.5). However, there was low saltation in 2013, 2016 and 2017 that was caused by high U_t, which was related to high vegetation components, while the low wind speed led to lower saltation in 2014.

4.2. Potential effects of wind-eroded coarse-textured topsoil on plant production

In the second part of this study, we compared the simulations of AGP_{act} between the actual condition and the wind-eroded scenario (Figure 4.2 and Table 3.3). We found that plant production in the wind-eroded topsoil decreased by 20.2% in the desert steppe (TsO) and slightly increased by 5.0% in the steppe (BU) during the critical growing seasons from 2002 to 2011. These results indicate that the effects of the coarse-textured topsoil on the plant production may change with variations in the Mongolian grasslands' climatic conditions.

The annual precipitation was lower at TsO (Figure 4.2–a1) (between 38.2 and 164.5 mm from 2002 to 2011). In the wind-eroded scenario and the actual condition, this

precipitation did not penetrate the deeper soil but was stored in the topsoil layer (Figure 4.2–a2). The coarse topsoil meant that the water holding capacity in the wind-eroded scenario was low, and the evapotranspiration was greater than in the actual condition (Figure 4.2–a3). Therefore, there was less soil moisture in the root-zone (0.1–0.3 m depth) in the wind-eroded scenario than in the actual condition (Figure 4.2–a4). Previous studies have stated that vegetation growth in arid ecosystems with low precipitation is mainly controlled by water (Noy-Meir, 1973). Field studies had shown that, when the available precipitation is less than 200 mm, the productivity of natural grass is low and do not differ significantly under different N fertilizer application rates (Kinugasa et al., 2012). Nandintsetseg and Shinoda (2011) showed that soil moisture is below the Mongolian mean and close to the wilting point throughout the year in the desert steppe. Therefore, the available soil water is the primary influence on plant production in arid ecosystems (Lauenroth and Sala, 1992). At TsO, plant production decreased in the wind-eroded scenario due to increased water stress, caused by an increase in evapotranspiration and reduced soil water in the root zoon (Figure 4.2–a5).

In contrast, at BU, the main reason for the slight increase in plant production was decreased water stress. As shown in Figure 4.2–b1, when the annual precipitation ranged from 89.2 to 250.4 mm (from 2002 to 2011), more precipitation penetrated the deeper soil in the wind-eroded scenario because of the lower water holding capacity and higher hydraulic conductivity in the wind-eroded topsoil (Figures 4.2–b2 and 4.2–b3). The evapotranspiration from the coarse topsoil in the wind-eroded scenario was lower than that from the loamy topsoil in the actual condition (Figure 4.2–b4). Together, these factors meant more water in the root-zone to facilitate plant growth (Figure 4.2–b5) in the wind-eroded scenario. Previous researchers have called this the inverse texture effect (e.g.,

Noy-Meir, 1973; Sala et al., 1988), and it has been observed in sandy regions with relatively high precipitation (< 300 mm). After adding equal amounts of water in experiments in a warm greenhouse, Alizai and Hulbert (1970) showed that evaporation is often greater from a loam bare soil than sand. Field studies (Sala et al., 1988; Yang et al., 2009) have shown that the plant production is higher in sandy soils with lower water holding capacity in wetter grasslands than in loamy soils with higher water holding capacity on the Tibetan Plateau and the Central Grassland region of America. Although the plant growth is limited by the available soil water in the semi-arid areas where inverse texture effects are apparent, it is more sensitive to nitrogen stress when there is enough soil water during the summer, as also reported elsewhere. Field-based studies (Hooper and Johnson, 1999) showed that plant production is limited by both water availability and nitrogen in a semi-arid region, and production responds positively to N additions as the water available increases. Also, Kinugasa et al. (2012) reported that when N is added to the wetter steppe soils at BU, it has more effect on plant production in wetter years (when the water stress is lower) than in drier years (when the water stress is higher).

As wind erosion processes, previous studies showed that there is a significant decrease in the proportion of fine particles in surface soil that are enriched by higher amounts of SOC and nutrients (Li et al., 2007, 2009; Yan et al., 2018), thereby likely causing a reduction in plant production. However, our results show that plant production reductions were mainly caused by increases in water stress in wind-eroded topsoil at both sites in the Mongolian grasslands. A field experiment in farmland in arid and semi-arid regions in Inner Mongolia showed that soil subjected to wind erosion since the 1980s was significantly coarser and drier than non-eroded land. Moreover, when high amounts of sand accumulate (72.6% sand), the average soil moisture content decreased significantly

(Zhao et al., 2006). These results imply that the soil water status may affect more than the soil nutrient pool in the wind-eroded coarse-textured topsoil in arid and semi-arid regions.

4.3. Interactions between wind erosion and ecosystem dynamics

The interactions between wind erosion and ecosystem dynamics are the complex system in drylands. Seasonal variations in land surface conditions affect the frequency and magnitude of wind erosion. Wind erosion, in turn, controls the redistribution of topsoil and the loss of nutrients, and thus affects the cycles of water, nutrients and C. In addition, increases in frequency and intensity of extreme events (e.g., drought and heat ware) and human activity (e.g., grazing) affect ecosystem dynamics. Nandintsetseg and Shinoda (2013) showed that the severity and frequency of growing-season droughts drove a reduction in plant production in Mongolia in the 2000s. Du et al. (2019) figured out that livestock grazing, one of the important human activity in arid and semi-arid regions, reduced vegetation coverage and biomass, and loosed topsoil. These affect erodibility by decreasing U_{t} and link to a remarkable increase in dust outbreak in Mongolia (Kurosaki et al., 2011).

In this study, we identify that plant life cycle and soil freeze–thaw processes are the critical factors for wind erosion in the dust source hotspot in Mongolia. Moreover, we suggest that the coarsening of topsoil by wind erosion reduces soil water storage capacity, and potentially affects the cycles of water and plant production. However, our study lacks comprehensive consideration in the impacts of wind erosion on the redistribution of topsoil. For example, we assumed a constant soil texture in this study but a real change in topsoil caused by wind erosion is dynamic. To deeply understand the interactions between wind erosion and ecosystem dynamics, we will develop a unique coupled model

in the future. Previous models (e.g., Mayaud et al., 2017; Zhang et al., 2020) have been established to simulate the interactions between wind erosion and ecosystem dynamics. However, they mainly focused on the relationships between physical sediment transport dynamics (i.e., erosion and deposition) and plant structure, and neglected how biogeochemical cycles are influenced under wind erosion. Therefore, based on our results, we propose that a new coupled model should focus on the effects of plant life cycles and soil freeze–thaw processes on wind erosion, and the relationships between wind erosion and the cycles of water, C and nutrients.

5. Conclusions

In this thesis, we investigated the relationships between wind erosion and ecosystem dynamics in the dust source hotspot in East Asia using a process-based ecosystem model (DAYCENT) and field observation dataset (e.g., weather, saltation and vegetation). There are two objectives in this study (Figure 1.1): (1) the impacts of land surface conditions on wind erosion, and (2) the potential impacts of wind erosion on ecosystem dynamics.

In the first part, we examined the impacts of land surface conditions on wind erosion during 2012–2017 in the desert steppe based on a combination of the unique 6-year field observation of saltation and simulated land surface elements by the DAYCENT model. Saltation tended to occur during February–June with strong western winds (>10 m s^{-1}). The highest frequency of saltation was in 2012 and 2015. U_t decreased with increasing soil temperature in spring (February–early May), and increased with increasing vegetation components of live and standing dead in early summer (late May–July). Our results suggest that saltation was possibly enhanced through soil freeze–thaw processes in spring, and suppressed through plant growth in addition to dead leaves, that are residues from the preceding summer. Moreover, a statistical model that predicts a realistic U_t is established and this model explains that frequent saltation in 2012 and 2015 resulted from a combination of frequent strong winds and a low U_t, which was related to changes in soil temperature and low standing dead and live grasses.

In the second part, we compared the plant production in the desert steppe and the steppe between the wind-eroded scenario and the actual condition using the DAYCENT model. For the wind-eroded topsoil, plant production decreased with increasing water stress in the desert steppe. However, it slightly increased in the steppe with decreasing water stress due to an inverse texture effect. Our results suggest soil water status may

affect more than the soil nutrient pool for decreases in plant production when the topsoil becomes coarser as the wind erosion progresses.

Generally, we highlight the importance of plant life cycle and soil freeze–thaw processes in wind erosion, and, in turn, how water stress, which is caused by the wind-eroded topsoil, significantly affects plant production. This outcome is expected to contribute to improve the accuracy of dust emission model and design effective land use management to control wind erosion in the Mongolian grasslands. Our study provides new insights into the relationships between wind erosion and ecosystem dynamics.

In the future, we will develop a DAYCENT-QF2003 coupled model to deeply understand the interactions between wind erosion and biogeochemical ecosystem dynamics under climate change and human activity. First, we are going to incorporate the DAYCENT into the QF2003 model to establish a daily high-solution dust-ecosystem simulation. Second, we are going to use the observational dataset in the dust source areas for inputting and validating simulations and thus estimate these interactions. Finally, we are going to apply the climate scenarios from the CMIP5 project and herding management scenarios to estimate these interactions under climate change and human activity in the future. This effort can contribute to an establishment of the long-term wind erosion monitoring system.

6. Figures

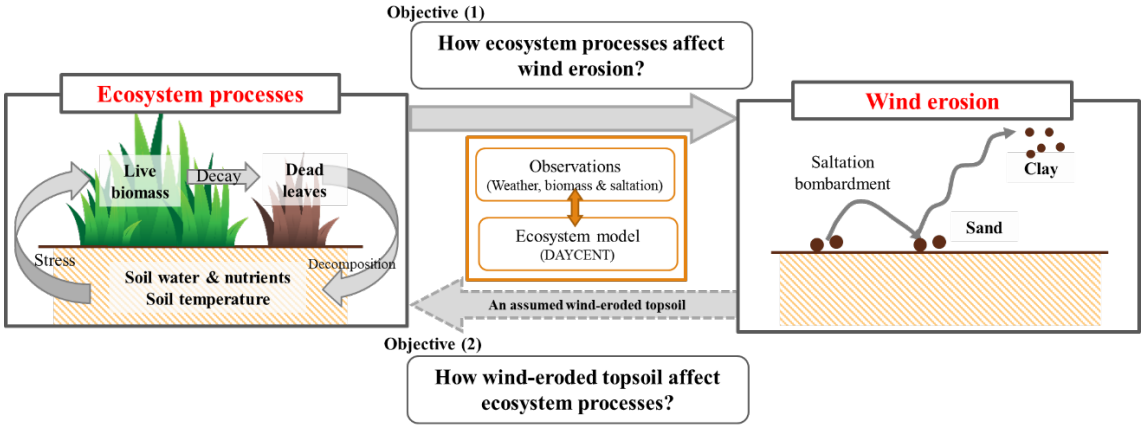

Figure 1.1 A schematic diagram of this study with two objectives.

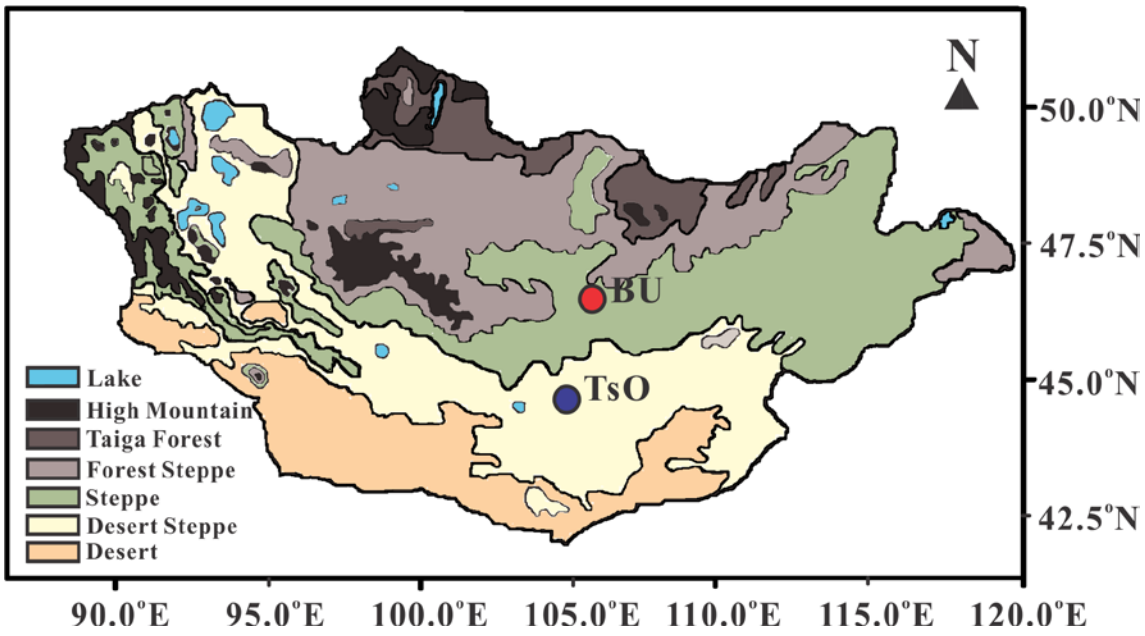

Figure 2.1 Locations of two study sites in the steppe (Bayan-Unjuul, BU) and the desert steppe (Tsogt-Ovoo, TsO), respectively, and vegetation zones in Mongolia.

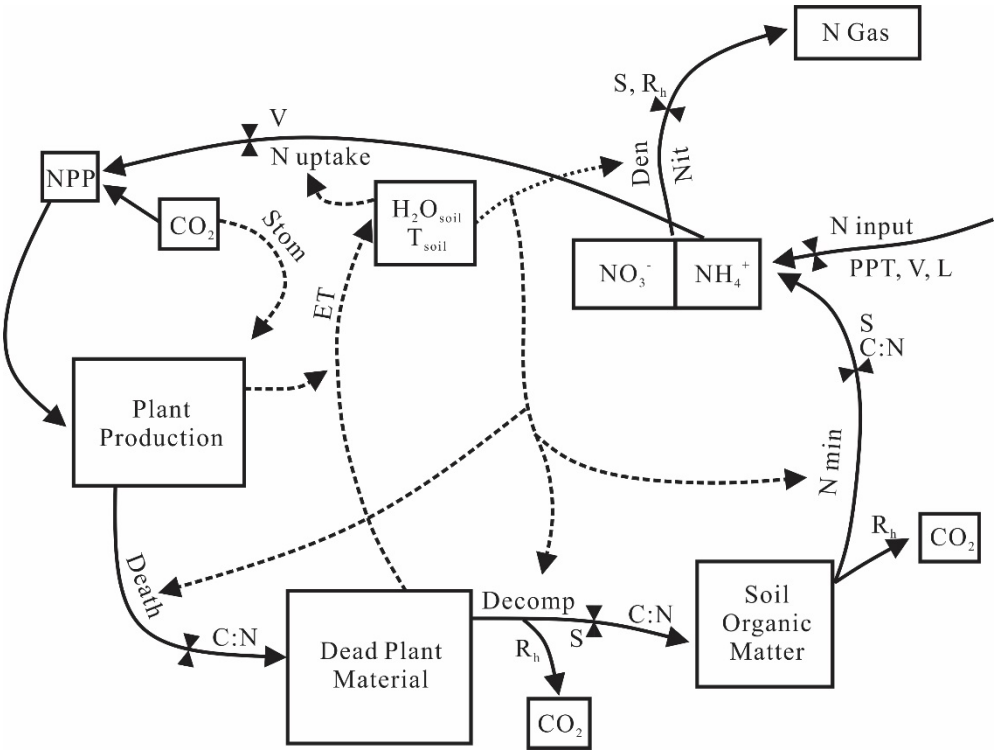

Figure 2.2 General flow diagram for the DAYCENT model (Modified by Parton et al., 1998). The solid lines indicate carbon and nitrogen flow. The dashed lines indicate feedbacks and information flows. H_2O_{soil} is soil water content; T_{soil} is soil temperature; S is soil texture; C:N is Carbon:Nitrogen ratio of material; V is vegetation type; SOM is soil organic matter; L is land use; Rh is heterotrophic respiration; N Gas is N_2O, NO_x and N_2; Stom is stomatal conductance; Death is plant component death; Decomp is decomposition; N inputs are N fixation, N deposition, and N fertilization; Nit is nitrification; Den is denitrification; N min is N mineralization; ET is evapotranspiration.

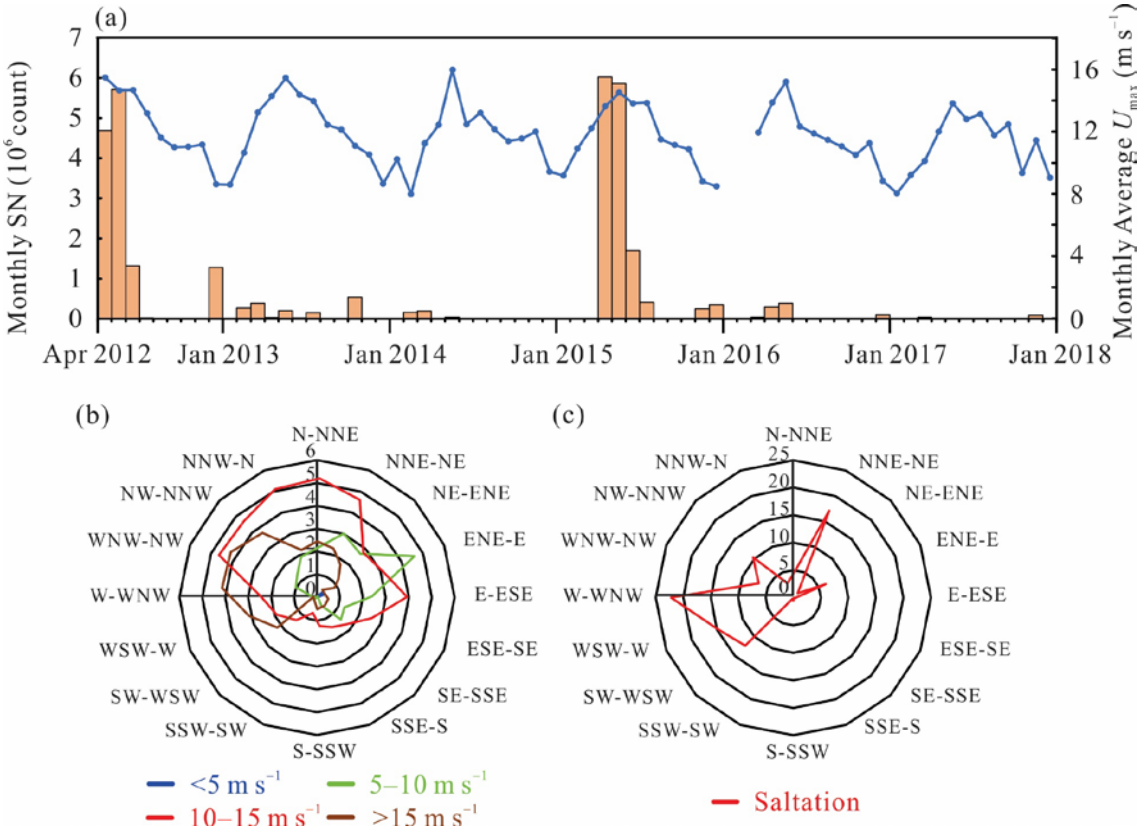

Figure 3.1 (a) Monthly total saltation number (SN) and averaged daily maximum wind speed (U_{max}) at TsO from April 2012 to December 2017. Frequency distributions (%) of wind direction (b) for four ranges (< 5, 5–10, 10–15, > 15 m s^{-1}) of U_{max} and (c) for daily total saltation number during saltation season (February–July) for 2012–2017.

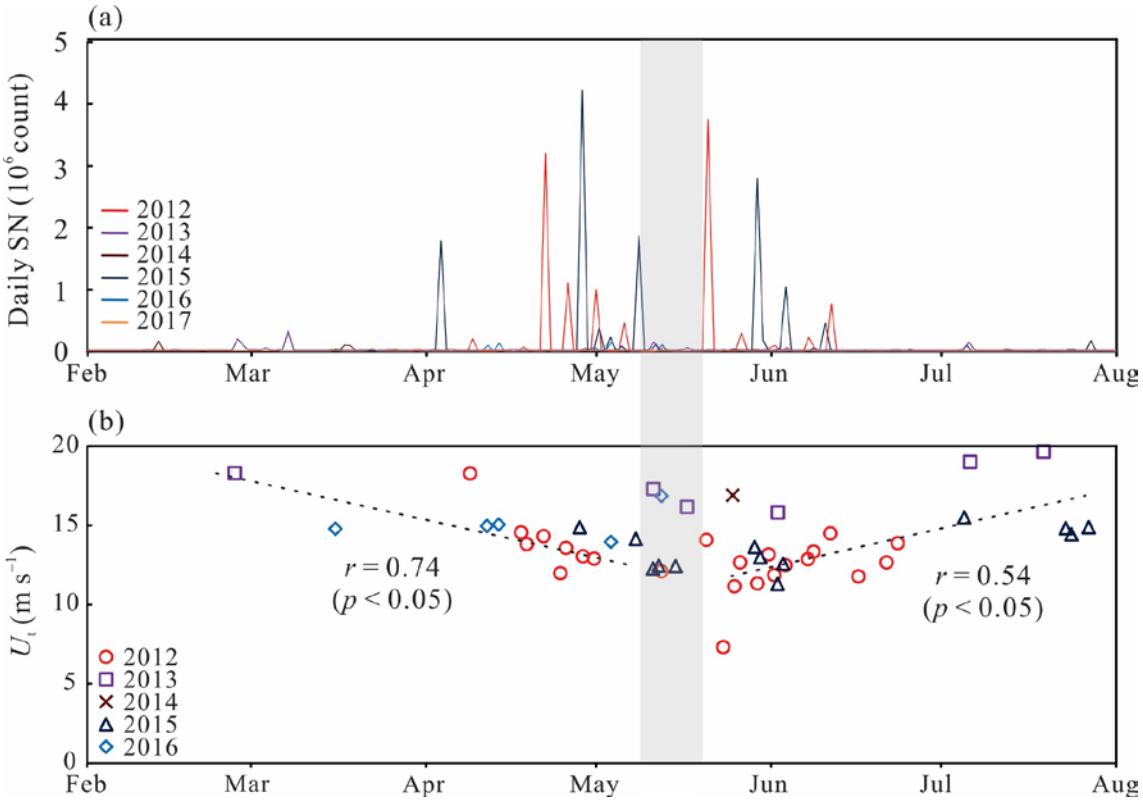

Figure 3.2 Distributions of daily (a) total saltation number (SN) and (b) the measurement-based threshold wind speed (U_t) during February–July for 2012–2017 at TsO. The grey bar illustrates the transitional period (mid-May) from the spring to early summer.

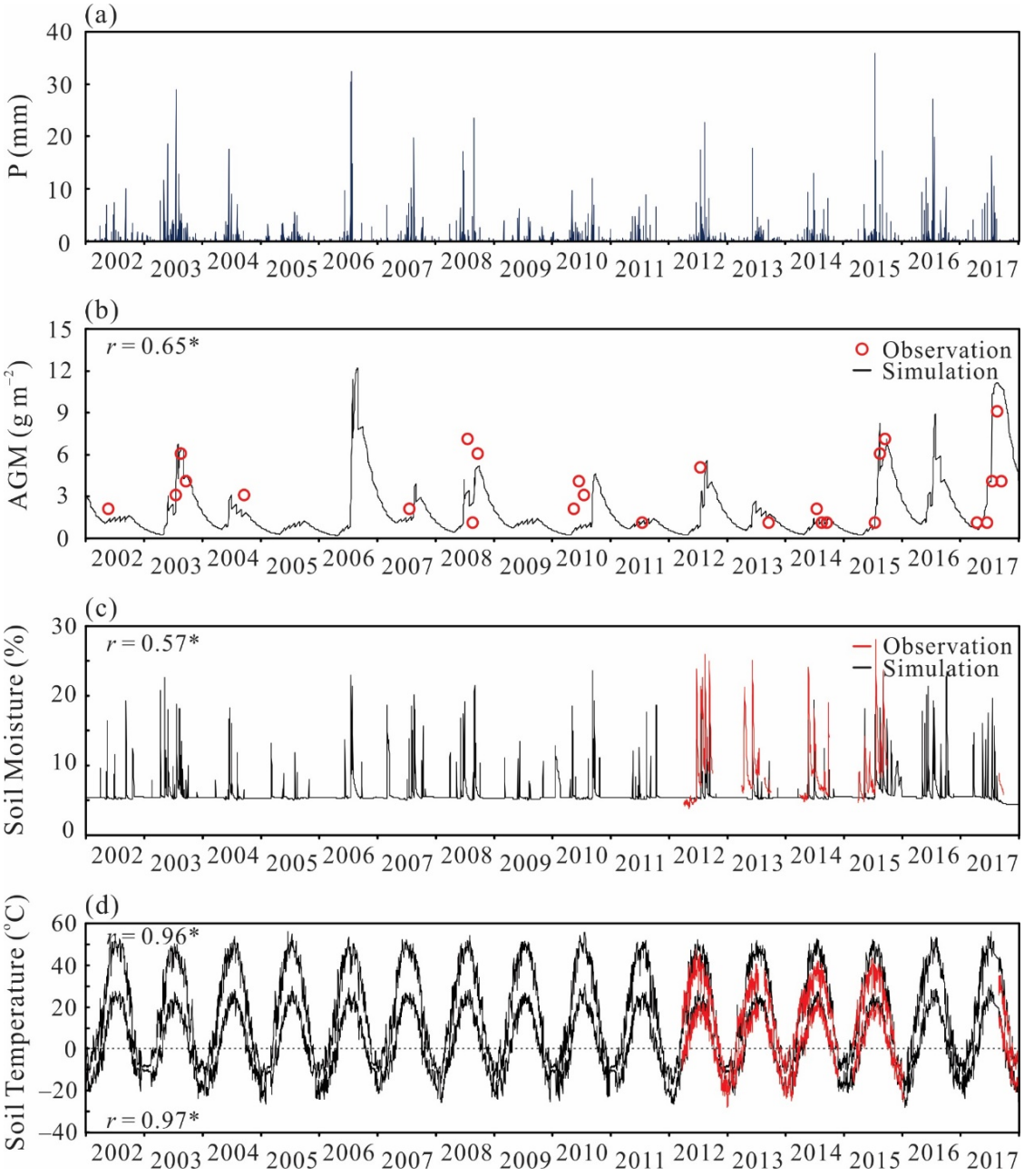

Figure 3.3 Daily (a) precipitation (P) and comparisons of the observed and simulated (b) aboveground vegetation mass (AGM) including live and standing dead grasses, (c) soil moisture at 0.025m depth, and (d) soil maximum and minimum temperatures at 0.025m depth from 2002 to 2017 at TsO. Asterisks (*) following the correlation coefficient (*r*) indicate significance at the 95% level.

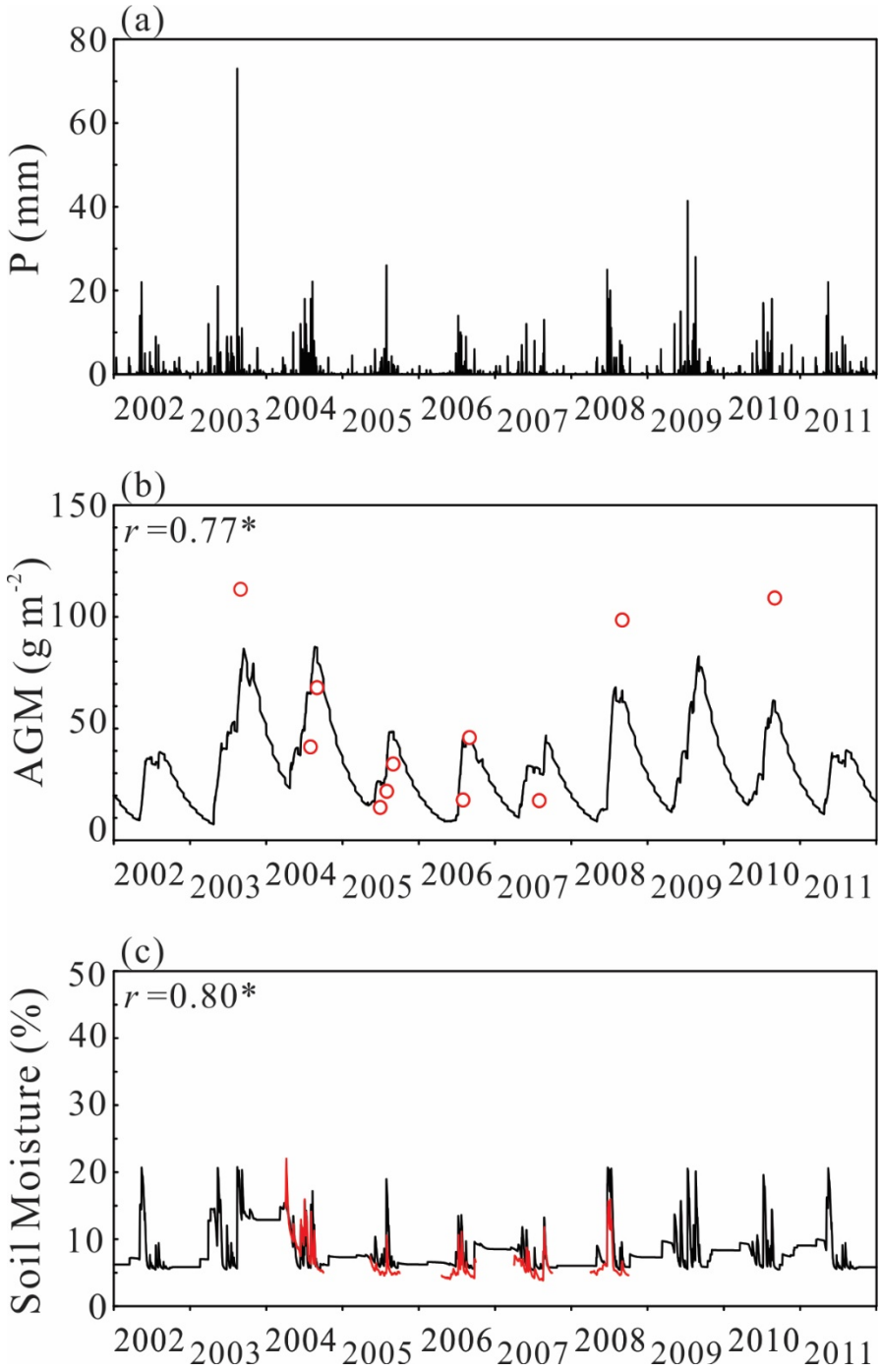

Figure 3.4 Daily (a) precipitation (P) and comparisons of the observed and simulated (b) aboveground vegetation mass (AGM) including live and standing dead grasses, and (c) soil moisture at 0.1m depth from 2002 to 2011 at BU. Asterisks (*) following the correlation coefficient (*r*) indicate significance at the 95% level.

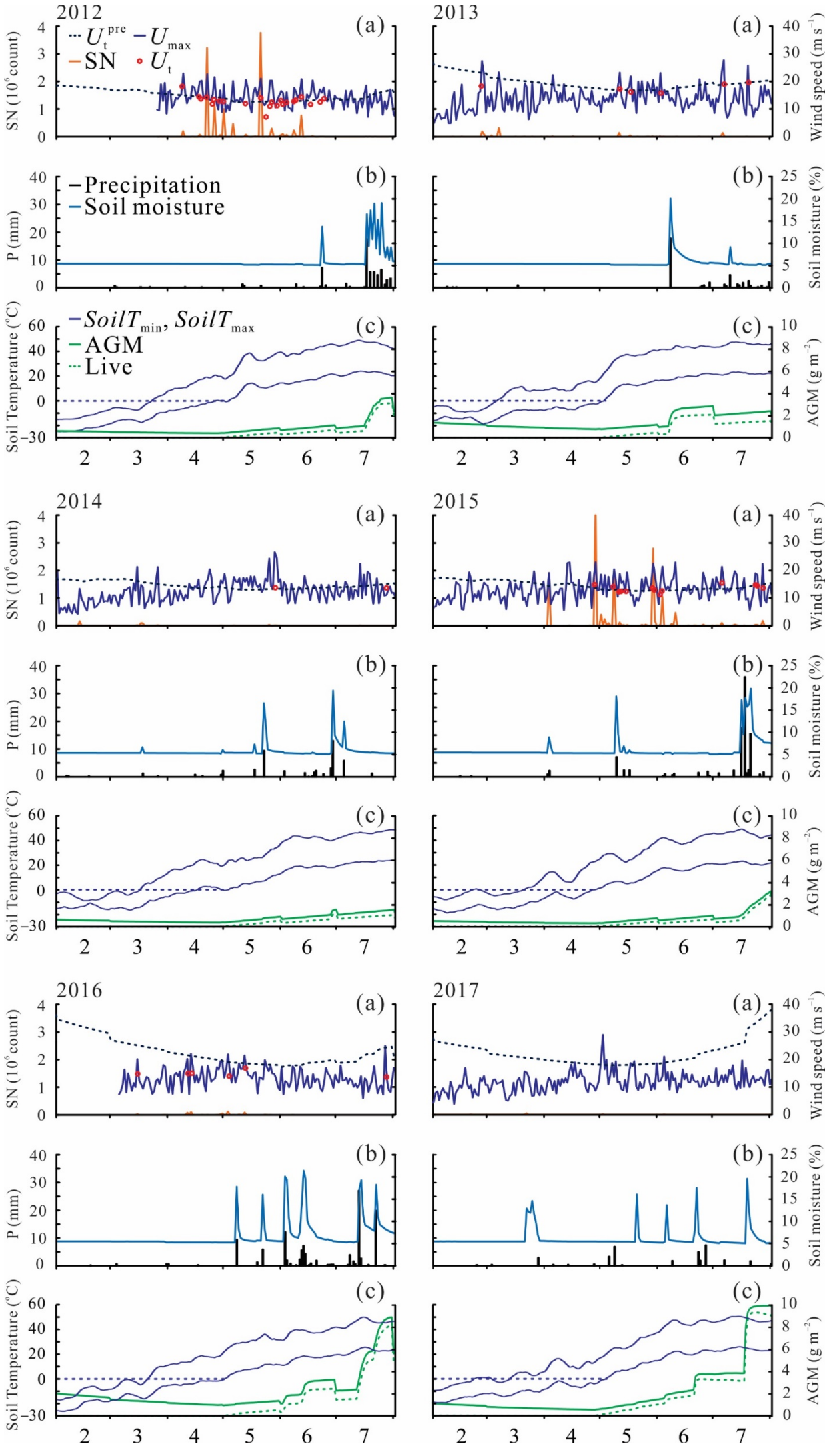
2012
2013
2014
2015
2016
2017
(a)
(b)
(c)
U_t^{pre}
U_{max}
SN
U_t
SN (10^6 count)
Wind speed (m s^{-1})
Precipitation
Soil moisture
P (mm)
Soil moisture (%)
$SoilT_{min}$, $SoilT_{max}$
AGM
Live
Soil Temperature (°C)
AGM (g m^{-2})

Figure 3.5 Daily variations in (a) total saltation number (SN) and the measurement-based and predicted threshold wind speed (U_t and $U_t{}^{pre}$) with maximum wind speed (U_{max}), (b) soil moisture with precipitation (P), and (c) 10-day moving average of surface soil maximum and minimum temperatures ($SoilT_{10\text{-day-min}}$ and $SoilT_{10\text{-day-min}}$) and aboveground vegetation mass (AGM, live and standing dead grasses) in saltation season (February–July) from 2012 to 2017.

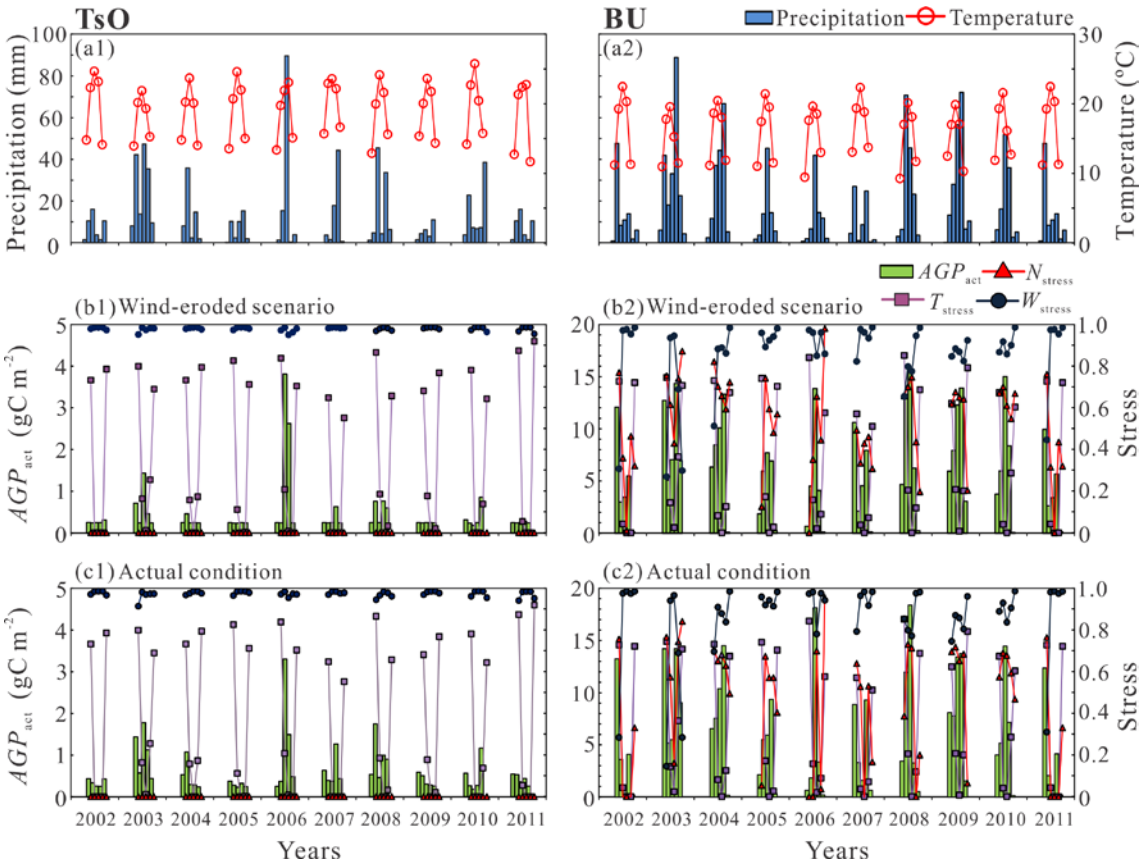

Figure 3.6 Monthly (a1 and a2) precipitation and air temperature and simulated AGP_{act}, W_{stress}, N_{stress}, and T_{stress} for (b1 and b2) the wind-eroded scenario and (c1 and c2) the actual condition during the growing season (May–September) from 2002 to 2011 at TsO and BU, respectively.

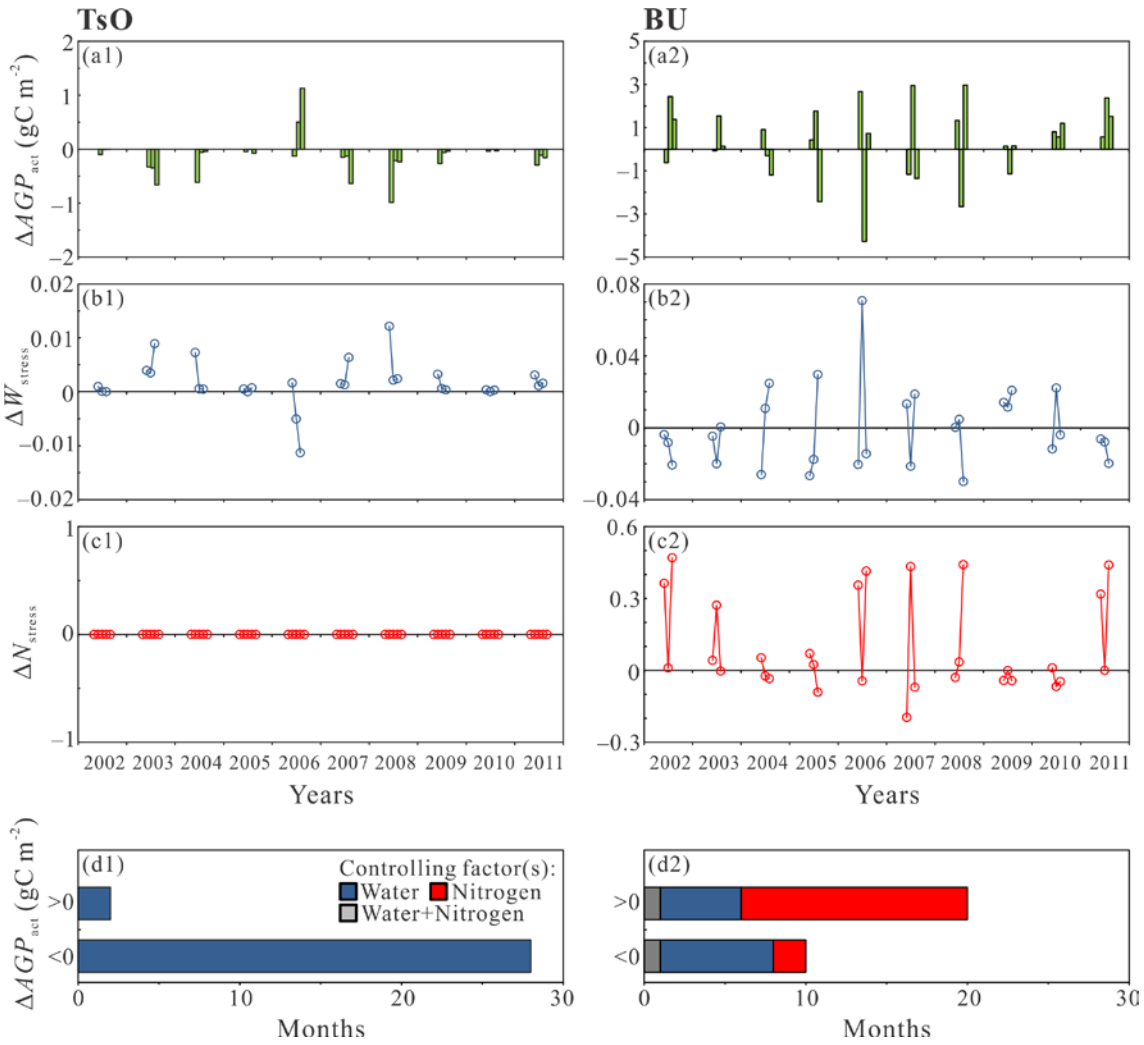

Figure 3.7 The monthly differences in (a1 and a2) AGP_{act}, (b1 and b2) W_{stress}, and (c1 and c2) N_{stress} between the actual condition and the wind-eroded scenario (ΔAGP_{act}, ΔW_{stress}, and ΔN_{stress}), and (d1 and d2) the number of months when plant growth experienced water and nitrogen stresses, during the critical growing season (June–August) from 2002 to 2011 at TsO and BU, respectively.

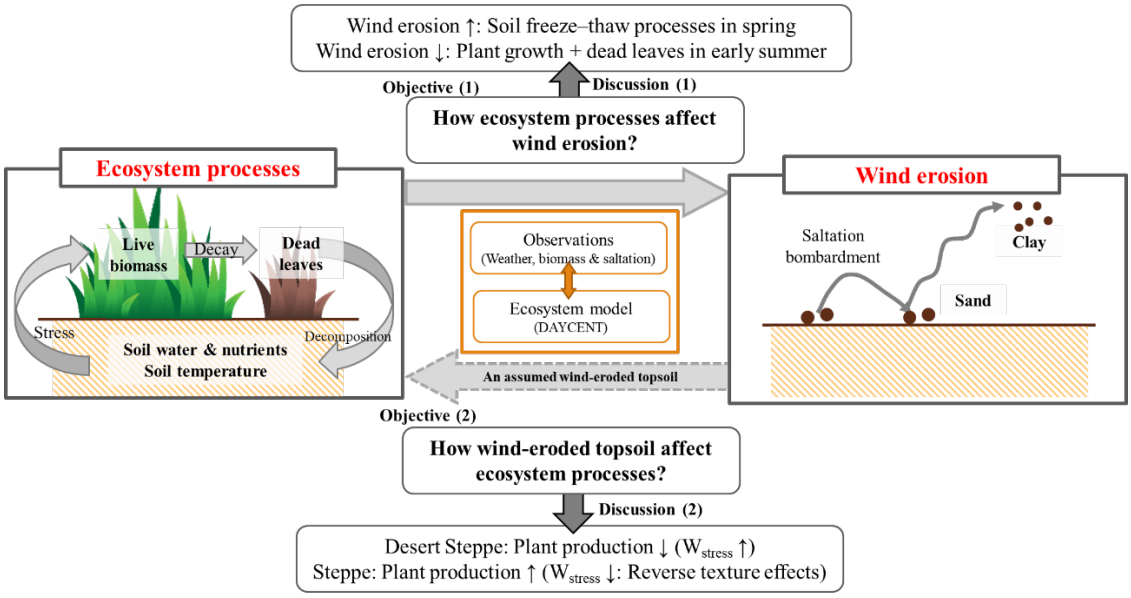

Figure 4.1 A schematic diagram of this study with two discussions.

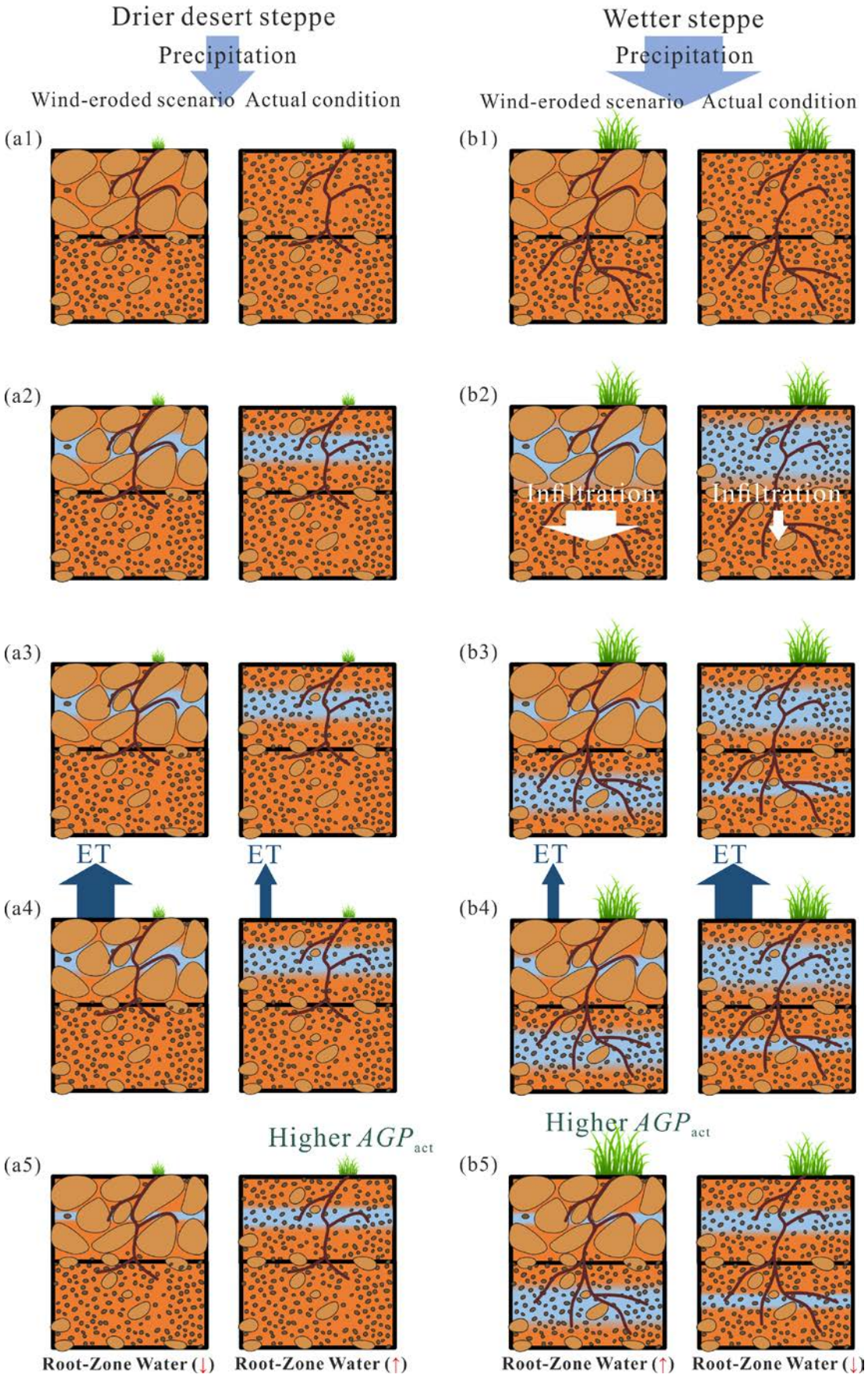
Drier desert steppe
Precipitation
Wind-eroded scenario
Actual condition
Wetter steppe
Precipitation
Wind-eroded scenario
Actual condition
(a1)
(b1)
(a2)
(b2)
Infiltration
Infiltration
(a3)
(b3)
ET
ET
ET
ET
(a4)
(b4)
Higher AGP_{act}
Higher AGP_{act}
(a5)
(b5)
Root-Zone Water (↓)
Root-Zone Water (↑)
Root-Zone Water (↑)
Root-Zone Water (↓)

Figure 4.2 Schematic representation of the different mechanisms that drove the changes in plant production in wind-eroded coarse-textured topsoil on the desert steppe (TsO, from a1 to a5) and the steppe (BU, from b1 to b5) because of the inverse texture effect. The different-sized (thick and thin) arrows indicate the magnitude (high and low) of the variables (precipitation, ET: evapotranspiration, and infiltration).

7. Tables

Table 2.1 Model parameterizations of the vegetation, soil and meteorological characteristics for the actual condition and the wind-eroded scenario.

No.	Parameter		Range (c)	TsO	BU
1	Fraction of clay in topsoil (0–0.1 m depth)	Actual condition	0.0–1.0	0.17 (a)	0.09 (a)
		Wind-eroded scenario	0.0–1.0	0.01	0.01
2	Fraction of sandy in topsoil (0–0.1 m depth)	Actual condition	0.0–1.0	0.64 (a)	0.65 (a)
		Wind-eroded scenario	0.0–1.0	0.99	0.99
3	Fraction of silt in topsoil (0–0.1 m depth)	Actual condition	0.0–1.0	0.19 (a)	0.24 (a)
		Wind-eroded scenario	0.0–1.0	0.00	0.00
4	Fraction of field capacity in topsoil (0–0.1 m depth)	Actual condition	0.0–1.0	0.23 (a)	0.21 (a)
		Wind-eroded scenario	0.0–1.0	0.09 (b)	0.09 (b)
5	Fraction of wilting point in topsoil (0–0.1 m depth)	Actual condition	0.0–1.0	0.10 (a)	0.07 (a)
		Wind-eroded scenario	0.0–1.0	0.02 (b)	0.02 (b)
6	Bulk density in topsoil (0–0.1 m depth) (g cm^{-3})	Actual condition	0.0–2.0	1.49 (a)	1.44 (a)
		Wind-eroded scenario	0.0–2.0	1.80 (b)	1.80 (b)
7	Potential aboveground monthly production for the C3 grasses (gC m^{-2})		100–300	100 (c)	300 (d)
8	Optimum temperature for C3 grasses (°C)		+10.0..+40.00	22.0 (c)	20.0 (c)
9	Maximum temperature for steppe (°C)		+20.0..+50.0	37.0 (c)	35.0 (c)
10	Physiological shutdown temperature for root death and change in shoot/root ratio of grass (°C)		–5.0..+5.0	2.0 (c)	2.0 (c)
11	Fraction of maximum shoot death rate at very dry soil conditions for steppe		0.0–1.0	0.2 (c)	0.2 (c)
12	Fraction of shoots which die during senescence month		0.4–1.0	0.95 (c)	0.95 (c)
13	Fraction of maximum root death rate at very dry conditions for steppe		0.0–1.0	0.05 (c)	0.05 (c)
14	Thickness of soil layers (m)			0.4 (a)	0.3 (a)
15	pH in topsoil (0–0.1 m depth)		0.0–15.0	8.2 (a)	6.5 (a)
16	Root depth (m)			0.4 (e)	0.4 (e)
17	Initial belowground biomass (g m^{-2})			50 (a)	200 (a)
18	Fraction of initial relative soil moisture content		0.0–1.0	0.16 (a)	0.16 (a)
19	Daily precipitation (mm)			(f)	(f)
20	Daily minimum air temperature (°C)			(f)	(f)
21	Daily maximum air temperature (°C)			(f)	(f)
22	Fraction of standing dead removed by a grazing event		0.0–1.0	0.05 (c)	0.01 (c)
23	Fraction content of feces		0.0–1.0	0.25 (c)	0.25 (c)
24	Fraction of live shoots removed by a grazing event		0.0–1.0	0.5 (c)	0.1 (c)

(a) Measured data at BU and TsO, mean parameters were related to the vegetation and soil types.
(b) Estimated data by Saxton's texture formula (Saxton and Rawls, 2006).
(c) Century user manual: http://www.nreal.colostat.edu/projects/century/ (Parton et al., 1992).
(d) IMH, 1996
(e) Nemoto, 2007
(f) The parameters varied with the season.

Table 3.1 Statistical analysis of simulated and observed parameters under the actual condition at TsO and BU sites.

Parameters	**TsO**				**BU**			
	Results of linear regression			D_{abs}	Results of linear regression			D_{abs}
	r	Slope	Intercept		*r*	Slope	Intercept	
Soil moisture	0.56*	0.9	0.9	2.6	0.80*	1.2	-1.3	1.8
AGM	0.60*	0.7	1.2	1.3	0.77*	1.5	-29.1	21.7

r: Pearson correlation coefficient; D_{abs}: Mean absolute deviation; * Significance at the 95% level.

Table 3.2 Correlation coefficients and the best models between U_t and the possible controlling land surface variables for the two periods (spring and early summer) of saltation season in 2012 and 2015[a]

Regressions	***Predictive Variables***	***Spring***	***Early summer***
Individual	AGM_{total}	0.22	0.11
	- Litter	0.14	−0.27
	- AGM	0.33	0.60***
	-Standing dead	0.39	0.82****
	- Live	−0.42	0.49**
	$SoilT_{\max}$	−0.60*	0.44*
	$SoilT_{\min}$	−0.65***	0.48*
	Soil moisture	−0.34	0.17
Best models	Spring: $SoilT_{\max}$, $SoilT_{\min}$	$U_t = -0.17 \times SoilT_{\min} + 14.20$	$U_t = 14.39 \times SD + 0.93 \times L + 9.81$
	Early summer: $SoilT_{\max}$, $SoilT_{\min}$, Standing dead (SD), Live (L)	$R^2_{adjusted}$ = 0.39 (p <0.005)	$R^2_{adjusted}$ = 0.70 (p <0.001)

[a] Rows correspond to stepwise multiple regressions with different sets of variables during distinct periods. Dependent variables are U_t in two periods of saltation season in 2012 and 2015.

$SoilT_{\max}$ and $SoilT_{\min}$: Moving averaged 10-day surface soil maximum and minimum temperatures.

AGMtotal: Aboveground total vegetation mass (live, standing dead, and litter).

AGM: Aboveground vegetation mass (live and standing dead).

* Significant at the 5% level.

** Significant at the 1% level.

***: Significant at the 0.5% level.

****: Significant at the 0.1% level.

Table 3.3 Simulated AGP_{act}, W_{stress}, N_{stress}, and T_{stress} values in May, July–August, and September for the actual condition and the wind-eroded scenario at TsO and BU.

	TsO						**BU**					
	Actual condition			Wind-eroded scenario			Actual condition			Wind-eroded scenario		
	May	Jun–Aug	Sep	May	Jun–Aug	Sep	May	Jun–Aug	Sep	May	Jun–Aug	Sep
AGP_{act} (gC m^{-2})	0.592	0.491	0.487	0.302	0.451	0.345	7.357	7.562	1.300	6.856	7.941	1.117
W_{stress} (Fraction, 0–1)	0.969	0.993	0.981	0.984	0.994	0.985	0.673	0.918	0.918	0.674	0.917	0.909
N_{stress} (Fraction, 0–1)	0.000	0.000	0.000	0.000	0.000	0.000	0.540	0.422	0.430	0.574	0.524	0.522
T_{stress} (Fraction, 0–1)	0.787	0.057	0.731	0.787	0.057	0.731	0.732	0.083	0.678	0.732	0.083	0.678

Table 3.4 The number of months when different controls affected plant production during the critical growing season (June–August) from 2002 to 2011

	ΔAGP_{act} **< 0**				ΔAGP_{act} **> 0**			
	$\Delta W > 0$	$\Delta W > 0$	$\Delta W > 0$	$\Delta W < 0$	$\Delta W > 0$	$\Delta W < 0$	$\Delta W < 0$	$\Delta W < 0$
	$\Delta N > 0$	$\Delta N = 0$	$\Delta N < 0$	$\Delta N > 0$	$\Delta N < 0$	$\Delta N > 0$	$\Delta N = 0$	$\Delta N < 0$
TsO	0	28	0	0	0	0	2	0
BU	1	0	7	2	5	14	0	1

ΔAGP_{act}, ΔW, and ΔN: The differences in the actual plant production, water stress, and nitrogen stress between the actual condition and the wind-eroded scenario.

References

Abulaiti, A., Kimura, R., 2011: Characteristics of the sand drifting of Tottori sand dune in springtime. *Sand Dune Res.*, **58(2)**, 31-40.

Abulaiti, A., Kimura, R., Shinoda, M., Kurosaki, Y., Mikami, M., Ishizuka, M., Tamada, Y., Nishihara, E., Gantsetseg, B., 2014: An observational study of saltation and dust emission in a hotspot of Mongolia. *Aeolian Res.*, **15**, 169-176.

Alizai, H.U., Hulbert, L.C., 1970: Effects of soil texture on evaporative loss and available water in semi-arid climates. *Soil Sci.*, **110(5)**, 328-332.

Bilbro, J. D., Fryrear, D. W., 1994: Wind erosion losses as related to plant silhouette and soil cover. *Agron. J.*, **86(3)**, 550-553.

Breshears, D. D., Whicker, J. J., Johansen, M. P., Pinder, J. E., 2003: Wind and water erosion and transport in semi-arid shrubland, grassland and forest ecosystems: Quantifying dominance of horizontal wind-driven transport. *Earth Surf. Processes Landforms*, **28(11)**, 1189-1209.

Byambakhuu, I., 2011: Study of ecohydrological responses to global warming and grazing pressure changes in Mongolian semi-arid region (Doctoral dissertation, PhD thesis, Graduate School of Life and Environ. Sciences, Univ. of Tsukuba, Japan).

Del Grosso, S.J., Parton, W.J., Mosier, A.R., Hartman, M.D., Keough, C.A., Peterson, G.A., Ojima, D.S., Schimel, D.S., 2001: Simulated effects of land use, soil texture, and precipitation on N gas emissions using DAYCENT. p. 413–431. In R.F. Follett and J.L. Hatfield (ed.) Nitrogen in the environment: Sources, problems, and management. Elsevier Science Publ., Amsterdam.

Del Grosso, S. J., Parton, W. J., Keough, C. A., Reyes-Fox, M., 2011: Special features of the DayCent modeling package and additional procedures for parameterization,

calibration, validation, and applications L.R. Ahuja, L. Ma (Eds.), Methods of Introducing System Models into Agricultural Research, American Society of Agronomy, Inc., Madison, WI (2011), pp. 155-176

Dordjgotov, D., 2003: Soil of Mongolia [in Mongolian], Admon, Ulaanbaatar.

Domby, C. W., Kohnke, H., 1955: The Effect of Freezing and Thawing on Structure of the Soil Surface 1. *Agron. J.*, **47(4)**, 175-177.

Eitzinger, J., Alexandrov, V., Cajic, V., Formayer, H., 2000: A site specific study on the potential range of climatic change impact on soil water balance and crop production under consideration of various models. In: Proceedings of the Third European Conference on Applied Climatology, ECAC'2000. Tools for the Environment and Man, Pisa, Italy, 2000. CD version, CNR-IATA, Institute of Agrometeorology and Environmental Analysis for Agriculture, Florence, Italy, 2000, 6 pp. ISBN 88-900502-0-9.

Fécan, F., Marticorena, B., Bergametti, G., 1998: Parametrization of the increase of the aeolian erosion threshold wind friction velocity due to soil moisture for arid and semi-arid areas. *Ann. Geophys.*, **17(1)**, 149-157.

Feng, X. M., Zhao, Y. S., 2011: Grazing intensity monitoring in Northern China steppe: Integrating CENTURY model and MODIS data. *Ecol. Indic.*, **11(1)**, 175-182.

Ferrick, M. G., Gatto, L. W., 2005: Quantifying the effect of a freeze–thaw cycle on soil erosion: laboratory experiments. *Earth Surf. Processes Landforms*, **30(10)**, 1305-1326.

Field, J. P., Belnap, J., Breshears, D. D., Neff, J. C., Okin, G. S., Whicker, J. J., Painter, T. H., Ravi, S., Reheis, M. C. Reynolds, R. L., 2010: The ecology of dust. *Front. Ecol. Environt.*, **8(8)**, 423-430.

Fryrear, D. W., Bilbro, J. D., 1994: Wind erosion control with residues and related

practices. Managing Agricultural Residues. Lewis, Boca Raton, FL, pp. 7–17.

Gilmanov, T. G., Parton, W. J., Ojima, D. S., 1997: Testing the 'CENTURY' ecosystem level model on data sets from eight grassland sites in the former USSR representing a wide climatic/soil gradient. *Ecol. Modell.*, **96(1-3)**, 191-210.

Han, L., Tsunekawa, A., Tsubo, M., 2010: Monitoring near-surface soil freeze–thaw cycles in northern China and Mongolia from 1998 to 2007. *Int. J. Appl. Earth Obs. Geoinf.*, **12(5)**, 375-384.

Han, L., Tsunekawa, A., Tsubo, M., 2011: Effect of frozen ground on dust outbreaks in spring on the eastern Mongolian Plateau. *Geomorphology*, **129(3-4)**, 412-416.

Hilbig, W., 1995: Vegetation of Mongolia. SPB Academic Pubishing.

Hoffmann, C., Funk, R., Wieland, R., Li, Y., Sommer, M., 2008: Effects of grazing and topography on dust flux and deposition in the Xilingele grassland, Inner Mongolia. *J. Arid Environ.*, **72(5)**, 792-807.

Holland, E. A., Parton, W. J., Detling, J. K., Coppock, D. L., 1992: Physiological responses of plant populations to herbivory and their consequences for ecosystem nutrient flow. *Am. Nat.*, **140(4)**, 685-706.

Hooper, D.U., Johnson, L., 1999: Nitrogen limitation in dryland ecosystems: responses to geographical and temporal variation in precipitation. *Biogeochemistry*, **46(1-3)**, 247-293.

Institute of Meteorology and Hydrology (IMH), 1996: Reference Book of Agrometeorological Meteorology [in Mongolian], NAMHEM, Ulaanbaatar.

Ishizuka, M., Mikami, M., Yamada, Y., Zeng, F., Gao, W., 2005: An observational study of soil moisture effects on wind erosion at a gobi site in the Taklimakan Desert. *J. Geophys. Res.*, **110(D18)**.

Ishizuka, M., Mikami, M., Leys, J., Yamada, Y., Heidenreich, S., Shao, Y., McTainsh, G. H., 2008: Effects of soil moisture and dried raindroplet crust on saltation and dust emission. *J. Geophys. Res.*, **113(D24)**.

Ishizuka, M., Mikami, M., Yamada, Y., Zeng, F., 2009: Threshold friction velocities of saltation sand particles for different soil moisture conditions in the Taklimakan Desert. *SOLA*, **5**, 184-187.

Ishizuka, M., Mikami, M., Yamada, Y., Kimura, R., Kurosaki, Y., Jugder, D., Gantsetseg, B., Cheng, Y., Shinoda, M., 2012: Does ground surface soil aggregation affect transition of the wind speed threshold for saltation and dust emission?. *SOLA*, **8**, 129-132.

Kassas, M., 1995: Desertification: a general review. *J. Arid Environ.*, **30(2)**, 115-128.

Kelly, R. H., Parton, W. J., Hartman, M. D., Stretch, L. K., Ojima, D. S., Schimel, D. S., 2000: Intra-annual and interannual variability of ecosystem processes in shortgrass steppe. *J. Geophys. Res.*, **105(D15)**, 20093-20100.

Kim, H., Choi, M., 2015: Impact of soil moisture on dust outbreaks in East Asia: Using satellite and assimilation data. *Geophys. Res. Lett.*, **42(8)**, 2789-2796.

Kim, J., 2008: Transport routes and source regions of Asian dust observed in Korea during the past 40 years (1965–2004). **Atmos. Environ.**, *42(19)*, 4778-4789.

Kimura, R., Shinoda, M., 2010: Spatial distribution of threshold wind speeds for dust outbreaks in northeast Asia. *Geomorphology*, **114(3)**, 319-325.

Kinugasa, T., Tsunekawa, A., Shinoda, M., 2012: Increasing nitrogen deposition enhances post-drought recovery of grassland productivity in the Mongolian steppe. *Oecologia*, **170(3)**, 857-865.

Kurosaki, Y., Mikami, M., 2004: Effect of snow cover on threshold wind velocity of dust

outbreak. *Geophys. Res. Lett.*, **31(3)**.

Kurosaki, Y., Mikami, M., 2007: Threshold wind speed for dust emission in East Asia and its seasonal variations. *J. Geophys. Res.*, **112(D17)**.

Kurosaki, Y., Shinoda, M., Mikami, M., 2011a: What caused a recent increase in dust outbreaks over East Asia?. *Geophys. Res. Lett.*, **38(11)**.

Kurosaki, Y., Shinoda, M., Mikami, M., Nandintsetseg, B., 2011b: Effects of soil and land surface conditions in summer on dust outbreaks in the following spring in a Mongolian grassland. *SOLA*, **7**, 69-72.

Kværnø, S. H., Øygarden, L., 2006: The influence of freeze–thaw cycles and soil moisture on aggregate stability of three soils in Norway. *Catena*, **67(3)**, 175-182.

Lal, R., 2003: Soil erosion and the global carbon budget. *Environ. Int.*, *29(4)*, 437-450.

Lal, R., 2011: Soil degradation by erosion. *Land Degrad. Dev.*, **12(6)**, 519-539.

Larney, F.J., Bullock, M.S., Janzen, H.H., Ellert, B.H., Olson, E.C., 1998: Wind erosion effects on nutrient redistribution and soil productivity. *J. Soil Water Conserv.*, **53(2)**, 133-140.

Lauenroth, W.K., Sala, O.E., 1992: Long–term forage production of North American shortgrass steppe. *Ecol. Appl.*, **2(4)**, 397-403.

Lee, J. J., Kim, C. H., 2012: Roles of surface wind, NDVI and snow cover in the recent changes in Asian dust storm occurrence frequency. *Atmos. Environ.*, **59**, 366-375.

LeBauer, D.S., Treseder, K.K., 2008: Nitrogen limitation of net primary productivity in terrestrial ecosystems is globally distributed. *Ecology*, **89(2)**, 371-379.

Lehrsch, G. A., 1998: Freeze-thaw cycles increase near-surface aggregate stability. *Soil Sci.*, **163(1)**, 63-70.

Lehrsch, G. A., Sojka, R. E., Carter, D. L., Jolley, P. M., 1991: Freezing effects on

aggregate stability affected by texture, mineralogy, and organic matter. *Soil Sci. Soc. Am. J.*, **55(5)**, 1401-1406.

Li, F., Zhao, L., Zhang, H., Zhang, T., Shirato, Y., 2004: Wind erosion and airborne dust deposition in farmland during spring in the Horqin Sandy Land of eastern Inner Mongolia, China. *Soil Tillage Res.*, **75(2)**, 121-130.

Li, J., Okin, G. S., Epstein, H. E., 2009: Effects of enhanced wind erosion on surface soil texture and characteristics of windblown sediments. *J. Geophys. Res. Biogeosci.*, **114(G2)**.

Li, J., Okin, G.S., Alvarez, L., Epstein, H., 2007: Quantitative effects of vegetation cover on wind erosion and soil nutrient loss in a desert grassland of southern New Mexico, USA. *Biogeochemistry*, **85(3)**, 317-332.

Li, J., Okin, G. S., Alvarez, L., & Epstein, H., 2008. Effects of wind erosion on the spatial heterogeneity of soil nutrients in two desert grassland communities. *Biogeochemistry*, **88(1)**, 73-88.

Li, X., Zhang, H., 2014: Soil moisture effects on sand saltation and dust emission observed over the Horqin Sandy Land area in China. *J. Meteorol. Res.*, **28(3)**, 444-452.

Lyles, L., Tatarko, J., 1986: Wind erosion effects on soil texture and organic matter. *J. Soil Water Conserv.*, **41(3)**, 191-193

Mandakh, N., Dash, D., Khaulenbek, A., 2007: Present status of desertification in Mongolia. *Geoecological issues in Mongolia*, **6**, 63-73.

Marticorena, B., Bergametti, G., 1995: Modeling the atmospheric dust cycle: 1. Design of a soil‐derived dust emission scheme. *J. Geophys. Res.*, **100(D8)**, 16415-16430.

Mayaud, J. R., Bailey, R. M., Wiggs, G. F., 2017: A coupled vegetation/sediment transport model for dryland environments. *J. Geophys. Res. Earth Surf.*, **122(4)**, 875-900.

Middleton, N., Thomas, D., 1997: World atlas of desertification. 2nd ed. Arnold, London.

Moriasi, D. N., Arnold, J. G., Van Liew, M. W., Bingner, R. L., Harmel, R. D., Veith, T. L., 2007: Model evaluation guidelines for systematic quantification of accuracy in watershed simulations. *Trans. ASABE*, **50(3)**, 885-900.

Munn, R. E., 1966: Descriptive micrometeorology. Academic Press, New York.

Nandintsetseg, B., Shinoda, M., 2011: Seasonal change of soil moisture in Mongolia: its climatology and modelling. *Int. J. Climatol.*, **31(8)**, 1143-1152.

Nandintsetseg, B., Shinoda, M., 2013: Assessment of drought frequency, duration, and severity and its impact on pasture production in Mongolia. *Nat. Hazards*, **66(2)**, 995-1008.

Nandintsetseg, B., Shinoda, M., 2015: Land surface memory effects on dust emission in a Mongolian temperate grassland. *J. Geophys. Res.*, **120(3)**, 414-427.

Nash, J. E., Sutcliffe, J. V., 1970: River flow forecasting through conceptual models part I—A discussion of principles. *J. Hydrol.*, **10(3)**, 282-290.

Natsagdorj, L., Jugder, D., Chung, Y. S., 2003: Analysis of dust storms observed in Mongolia during 1937–1999. *Atmos. Environ.*, **37(9-10)**, 1401-1411.

Noy-Meir, I., 1973: Desert ecosystems: environment and producers. *Annu. Rev. ecol. Syst.*, **4(1)**, 25-51.

Ojima, D. S., Dirks, B. O., Glenn, E. P., Owensby, C. E., Scurlock, J. O., 1993: Assessment of C budget for grasslands and drylands of the world. *Water Air Soil Pollut.*, **70(1-4)**, 95-109.

Ojima, D. S., Corell, R. W., 2009: Managing grassland ecosystems under global environmental change: Developing strategies to meet challenges and opportunities of global change. In Franzluebbers AJ (ed) Farming With Grass: Achieving Sustainable

Mixed Agricultural Landscapes. Soil and Water Conservation Society, Ankeny, pp 146–155.

Okin, G.S., Mahowald, N., Chadwick, O.A., Artaxo, P., 2004: Impact of desert dust on the biogeochemistry of phosphorus in terrestrial ecosystems. *Glob. Biogeochem. Cycles*, **18(2)**.

Owen, P. R., 1964: Saltation of uniform grains in air. *J. Fluid Mech.*, **20(2)**, 225-242.

Oztas, T., Fayetorbay, F., 2003: Effect of freezing and thawing processes on soil aggregate stability. *Catena*, **52(1)**, 1-8.

Parton, W. J., 1984: Predicting soil temperatures in a shortgrass steppe. *Soil Sci.*, **138(2)**, 93-101.

Parton, W. J., McKeown, B., Kirchner, V., Ojima, D. S., 1992: CENTURY Users Manual. Colorado State University NREL Publication, Fort Collins, CO.

Parton, W. J., Scurlock, J. M. O., Ojima, D. S., Schimel, D. S., Hall, D. O., Scopegram Group Members, 1995: Impact of climate change on grassland production and soil carbon worldwide. *Glob. Chang. Biol.*, **1(1)**, 13-22.

Parton, W. J., Hartman, M., Ojima, D., Schimel, D., 1998: DAYCENT and its land surface submodel: description and testing. *Global Planet. Change*, **19(1-4)**, 35-48.

Pawluk, S., 1988: Freeze-thaw effects on granular structure reorganization for soil materials of varying texture and moisture content. *Can. J. Soil Sci.*, **68(3)**, 485-494.

Penman, H. L., 1948: Natural evaporation from open water, bare soil and grass. *Proc. Roy. Soc. London Ser. A.*, **193(1032)**, 120-145.

Pi, H., Sharratt, B., 2019: Threshold Friction Velocity Influenced by the Crust Cover of Soils in the Columbia Plateau. *Soil Sci. Soc. Am. J.*, **83(1)**, 232-241.

Ravi, S., Breshears, D.D., Huxman, T.E., D'Odorico, P., 2010: Land degradation in

drylands: Interactions among hydrologic–aeolian erosion and vegetation dynamics. *Geomorphology*, **116(3)**, 236-245.

Ravi, S., D'Odorico, P., Breshears, D. D., Field, J. P., Goudie, A. S., Huxman, T. E., Li, J., Okin, G. S., Swap, R. J., Thomas, A. D., Van Pelt, S., Whicker, J. J., Zobeck, T. M., 2011: Aeolian processes and the biosphere. *Rev. Geophys.*, **49(3)**.

Ritter, A., Muñoz-Carpena, R., 2013: Performance evaluation of hydrological models: Statistical significance for reducing subjectivity in goodness-of-fit assessments. *J. Hydrol.*, **480**, 33-45.

Sala, O.E., Parton, W.J., Joyce, L.A., Lauenroth, W.K., 1988: Primary production of the central grassland region of the United States. *Ecology*, **69(1)**, 40-45.

Saxton, K.E., Rawls, W.J., 2006: Soil water characteristic estimates by texture and organic matter for hydrologic solutions. *Soil Sci. Soc. Am. J.*, **70(5)**, 1569-1578.

Shao, Y., 2001: A model for mineral dust emission. *J. Geophys. Res.*, **106(D17)**, 20239-20254.

Schulze, E.D., Beck, E., Müller-Hohenstein, K., 2005: Environment as Stress Factor: Stress Physiology of Plants. *Plant. Ecol.*, **702(9)**, 506.

Shao, Y., 2004: Simplification of a dust emission scheme and comparison with data. *J. Geophys. Res.*, **109(D10)**.

Shao, Y., Mikami, M., 2005: Heterogeneous saltation: Theory, observation and comparison. *Boundary Layer Meteorol.*, **115(3)**, 359-379.

Shao, Y., Dong, C. H., 2006: A review on East Asian dust storm climate, modelling and monitoring. *Global Planet. Change*, **52(1-4)**, 1-22.

Shao, Y., 2008: Physics and Modelling of Wind Erosion. 2nd ed. Springer, Heidelberg.

Shao, Y., Wyrwoll, K.H., Chappell, A., Huang, J., Lin, Z., McTainsh, G.H., Mikami, M.,

Tanaka, T.Y., Wang, X., Yoon, S., 2011: Dust cycle: An emerging core theme in Earth system science. *Aeolian Res.*, **2(4)**, 181-204.

Shinoda, M., Kimura, R., Mikami, M., Tsubo, M., Nishihara, E., Ishizuka, M., Yamada, E., Munkhtsetseg, E., Jugder, D., Kurosaki, Y., 2010: Characteristics of dust emission in the Mongolian steppe during the 2008 DUVEX intensive observational period. *SOLA*, **6**, 9-12.

Shinoda, M., Gillies, J. A., Mikami, M., Shao, Y., 2011: Temperate grasslands as a dust source: Knowledge, uncertainties, and challenges. *Aeolian Res.*, **3(3)**, 271-293.

Shinoda, M., Nandintsetseg, B., Nachinshonhor, U.G., Komiyama, H., 2014: Hotspots of recent drought in Asian steppes. *Reg. Environ. Chang.*, **14(1)**, 103-117.

Song, H., Wang, K., Zhang, Y., Hong, C., Zhou, S., 2017: Simulation and evaluation of dust emissions with WRF-Chem (v3. 7.1) and its relationship to the changing climate over East Asia from 1980 to 2015. *Atmos. Environ.*, **167**, 511-522.

Sterk, G., Parigiani, J., Cittadini, E., Peters, P., Scholberg, J., Peri, P., 2012: Aeolian sediment mass fluxes on a sandy soil in Central Patagonia. *Catena*, **95**, 112-123.

Sugimoto, N., Hara, Y., Yumimoto, K., Uno, I., Nishikawa, M., Dulam, J., 2010: Dust emission estimated with an assimilated dust transport model using lidar network data and vegetation growth in the Gobi desert in Mongolia. *SOLA*, **6**, 125-128.

Sugita, M., Asanuma, J., Tsujimura, M., Mariko, S., Lu, M., Kimura, F., Azzaya, D., Adyasuren, T., 2007: An overview of the rangelands atmosphere–hydrosphere–biosphere interaction study experiment in northeastern Asia (RAISE). *J. hydrol.*, **333(1)**, 3-20.

Szymańska, R., Ślesak, I., Orzechowska, A., Kruk, J., 2017: Physiological and biochemical responses to high light and temperature stress in plants. *Environ. Exp. Bot.*,

139, 165-177.

Tanaka, T. Y., Chiba, M., 2005: Global simulation of dust aerosol with a chemical transport model, MASINGAR. *J. Meteorol. Soc. Japan*, **83**, 255-278.

Throop, H. L., Holland, E. A., Parton, W. J., Ojima, D. S., Keough, C. A., 2004: Effects of nitrogen deposition and insect herbivory on patterns of ecosystem–level carbon and nitrogen dynamics: results from the CENTURY model. *Glob. Chang. Biol.*, **10(7)**, 1092-1105.

United Nations Environment Programme, 1997: World Atlas of Desertification, 2nd ed., edited by N. J. Middleton and D. S. G. Thomas, Edward. Arnold, London.

Urgamal, M., Oyuntsetseg, B., 2017: Atlas of the endemic vascular plants of Mongolia. Bembi San, Ulaanbaatar.

Van Oost, K., Quine, T.A., Govers, G., De Gryze, S., Six, J., Harden, J.W., Ritchie, J.C., McCarty, G.W., Heckrath, G., Kosmas, C., Giraldez, J.V., Marques da Silva, J.R., Merckx, R., 2007: The impact of agricultural soil erosion on the global carbon cycle. *Science*, **318(5850)**, 626-629.

Wei, X., Huang, C., Wei, N., Zhao, H., He, Y., Wu, X., 2019: The impact of freeze–thaw cycles and soil moisture content at freezing on runoff and soil loss. *Land Degrad. Dev.*, **30(5)**, 515-523.

Yan, Y., Wang, X., Guo, Z., Chen, J., Xin, X., Xu, D., Yan, R., Chen, B., Xu, L., 2018: Influence of wind erosion on dry aggregate size distribution and nutrients in three steppe soils in northern China. *Catena*, **170**, 159-168.

Yang, X., Zhou, C., Huo, W., Yang, F., Liu, X., Mamtimin, A., 2019: A study on the effects of soil moisture, air humidity, and air temperature on wind speed threshold for dust emissions in the Taklimakan Desert. *Nat. Hazards*, **97(3)**, 1069-1081.

Yang, Y., Fang, J., Pan, Y., Ji, C., 2009: Aboveground biomass in Tibetan grasslands. *J. Arid Environ.*, **73(1)**, 91-95.

Yao, S., Zhang, T., Zhao, C., Liu, X., 2013: Saturated hydraulic conductivity of soils in the Horqin Sand Land of Inner Mongolia, northern China. Environ. *Monit. Assess.*, **185(7)**, 6013-6021.

Yin, J., D'Odorico, P., Porporato, A., 2019: Soil Moisture Dynamics in Water-Limited Ecosystems, in: D'Odorico, P., Porporato, A., Runyan, C.W. (Eds.), Dryland Ecohydrology. Springer, Cham, pp. 31-48.

Žabenská, A., Dumbrovský, M., 2015: Changes of soil aggregate stability as a result of the effect of freeze-thaw cycles. *Acta Univ. Agric. Silvic. Mendelianae Brun.*, **63(4)**, 1211-1218.

Zhang, J., 2020: A new ecological-wind erosion model to simulate the impacts of aeolian transport on dryland vegetation patterns. *Acta Ecologica Sinica.*,

Zhao, H., Yi, X., Zhou, R., Zhao, X., Zhang, T, Drake, S., 2006: Wind erosion and sand accumulation effects on soil properties in Horqin Sandy Farmland, Inner Mongolia. *Catena*, **65(1)**, 71-79.